




Cubic anisotropy of hole Zeeman splitting in semiconductor nanocrystals

M. A. Semina ^{*}, A. A. Golovatenko , and A. V. Rodina
Ioffe Institute, 194021, St.-Petersburg, Russia

 (Received 17 October 2023; revised 27 November 2023; accepted 28 November 2023; published 15 December 2023)

We study theoretically cubic anisotropy of Zeeman splitting of a hole confined in a semiconductor nanocrystal. This anisotropy originates from three contributions: crystallographic cubically symmetric spin and kinetic energy terms in the bulk Luttinger Hamiltonian and the spatial wave function distribution in a cube-shaped nanocrystal. From symmetry considerations, an effective Zeeman Hamiltonian for the hole's lowest even state is introduced, containing a spherically symmetric and a cubically symmetric term. The values of these terms are calculated numerically for spherical and cube-shaped nanocrystals as functions of the Luttinger Hamiltonian parameters. We demonstrate that the cubic shape of the nanocrystal and the cubic anisotropy of hole kinetic energy (so-called valence band warping) significantly affect effective g factors of hole states. In both cases, the effect comes from the cubic symmetry of the hole wave functions in a zero magnetic field. Estimations for the effective g factor values in several semiconductors with zinc-blende crystal lattices are made. Possible experimental manifestations and potential methods for measuring of the cubic anisotropy of the hole Zeeman splitting are suggested.

DOI: [10.1103/PhysRevB.108.235310](https://doi.org/10.1103/PhysRevB.108.235310)

I. INTRODUCTION

Today state-of-the-art methods of chemical synthesis make it possible to grow semiconductor colloidal quantum dots or nanocrystals (NCs) with desired shapes on demand. For example, typical II-VI semiconductor (CdS, CdSe, and CdTe) NCs tend to have a shape close to spherical [1] and lead-halide perovskite NCs naturally grow in the form of cubes [2]. However, by choosing special synthesis conditions, it is possible to control the shape of NCs. It is known that CdSe NCs can be obtained in the form of nanorods, nanoplatelets, tetrapods [1]. Recently, cube-shaped CdSe and CdS NCs with zinc-blende crystal structure have been synthesized [3,4]. This diversity of NC shapes is interesting not only from the point of view of the capabilities of modern methods of colloidal synthesis, but also because it opens the possibility of studying the effect of the NC shape on the physical properties of charge carriers confined in NCs.

The dependence of size quantization energy on NC shape is known from textbooks, but there are more subtle effects, for example, the strong dependence of the spin properties of localized charge carriers on NC size and symmetry. The enduring interest in the spin properties of charge carriers localized in NCs is associated with the possibility of their application in spintronics and quantum computing, as it was proposed in the Loss-DiVincenzo paper [5] for electrons and was further generalized for holes [6,7]. The main searches in this direction are based on the use of direct band gap semiconductors of type III-V (GaAs) or II-VI (CdSe, CdTe), which have zinc-blende crystal structure.

These semiconductor materials are characterized by a strong spin-orbit interaction. For electrons in the S -type con-

duction band, the spin-orbit interaction results in deviation of the electron g factor from the free electron g factor, as it was shown in the Roth-Lax-Zwerdling paper for bulk semiconductors [8]. In small NCs, spatial localization of electrons decreases the spin-orbit interaction effect on electron g factor, so that its value tends to the free electron g factor [9–11]. In spherically and cubically symmetric confining potentials, the splitting of electron spin sublevels is described by an isotropic g factor.

The topmost valence band in these materials has a P -type symmetry. Due to the strong spin-orbit interaction, the valence band splits into two subbands with the total angular momentum of a hole $J = 3/2$ and $1/2$. The splitting between these subbands reaches hundreds of meVs. The ground hole state in these materials corresponds to the fourfold degenerate valence subband with $J = 3/2$. The calculation of the hole g factor in this case within the kp -method for bulk semiconductors was first performed by Luttinger [12]. He showed that the cubic symmetry of the crystal lattice leads to two additional contributions to the splitting of hole states in a magnetic field. The first contribution is due to the valence band warping, and the second to the cubic-symmetric invariant $\propto J^3 B$. These contributions results in dependence of the hole spin splitting in an external magnetic field on the angle between crystal axes and magnetic field. The influence of these contributions on a hole localized at different types of acceptors in GaAs was studied in Ref. [13]. It was found that the contribution to the hole spin splitting from the cubically symmetric term of the Luttinger Hamiltonian can be comparable to the spherically symmetric contribution [13].

However, often the contribution originating from the cubic symmetry of the crystal lattice is neglected, and the hole g factor is calculated in the spherical approximation of the Luttinger Hamiltonian [14,15]. This approach was widely used for interpretation of magneto-optical experiments on colloidal

*semina@mail.ioffe.ru

NCs [16–21]. To the best of our knowledge, the applicability of such an approach has not been assessed yet. Since the cubically symmetric contribution to the effective g factor of a hole localized on an acceptor [13] is not negligible, one can expect the similar result for a hole localized in a NC.

For instance, accounting for the cubic symmetry of a crystal lattice becomes crucial for understanding the spin properties of holes in thin quantum wells. Due to a large energy splitting of the localized states of the light and heavy holes in thin quantum wells, the transverse g factor of the heavy hole turns out to be identically equal to zero if one neglects the cubic symmetry of the crystal lattice. As a result, no spin precession of a heavy hole should be observed, which is not the case [22–24]. It was shown in [22] that accounting for the crystal lattice cubic symmetry in the form of the Hamiltonian term $\propto J^3 B$ results in the heavy hole having a nonzero transverse g factor, which explains experimental findings.

The effect of cubic symmetry on the spin splitting of a localized hole originates not only from the crystal lattice, but also from the confining potential symmetry [11]. Such a potential does not exist naturally in bulk semiconductors, but has been realized recently in cube-shaped CdSe NCs [3,4]. Thus it is interesting to reveal the effect of NC shape on hole spin splitting by comparing it in spherical and cube-shaped NCs.

In this paper, we study theoretically the spin splitting of holes in NCs of spherical and cubic shape in an applied magnetic field. We analyze and compare contributions of both the cubic symmetry of a semiconductor crystal structure and a NC's shape to hole spin splitting in an external magnetic field. It is found that in cube-shaped NCs, both contributions to the effective hole g factor are comparable with each other, and, although smaller, not negligible as compared to the isotropic contribution. We propose possible experimental manifestations of the cubically symmetric contribution to the hole spin splitting.

The paper is organized as follows. In Sec. II, we introduce the form of the hole effective Zeeman Hamiltonian in an external magnetic field from symmetry consideration. In Secs. III A and III B, we present results of calculations of hole Zeeman splitting without accounting for valence band warping in spherical and cube-shaped NCs. In Sec. III C, we analyze the contribution from valence band warping on NC of both shapes. In Sec. IV, we discuss possible experimental manifestations of the cubic anisotropy of hole Zeeman splitting.

II. SYMMETRY CONSIDERATION

We consider a hole from the top of the valence band in NCs based on semiconductors with a zinc-blende crystal lattice and a strong spin-orbit interaction. For a hole localized in an external potential $V_{\text{ext}}(\mathbf{r})$, and in the presence of an applied magnetic field, the Hamiltonian takes form:

$$\widehat{H} = \widehat{H}_L + \widehat{H}_Z + \widehat{H}_B + V_{\text{ext}}(\mathbf{r}). \quad (1)$$

The dispersion of hole states from the top of the valence band is described by the four-band Luttinger Hamiltonian \widehat{H}_L

[12,25]:

$$\widehat{H}_L = \frac{\hbar^2}{2m_0} \left[\left(\gamma_1 + \frac{5}{2}\gamma_2 \right) k^2 - 2\gamma_2 \sum_{\alpha} J_{\alpha}^2 k_{\alpha}^2 - 2\gamma_3 \sum_{\alpha \neq \beta} \{J_{\alpha} J_{\beta}\} \{k_{\alpha} k_{\beta}\} \right], \quad \alpha, \beta = x, y, z. \quad (2)$$

Here, the operator \mathbf{J} is the hole internal angular momentum operator, for the Γ_8 valence subband $J = 3/2$, $\gamma_1, \gamma_2, \gamma_3$ are Luttinger parameters, k_{α} are the hole wave vector components, and $\{ab\} = (ab + ba)/2$. The components of the wave vector k_{α} and pseudovector J_{α} transform according to the irreducible representation Γ_8 of the point group O_h or T_d . The Luttinger Hamiltonian (2) comprising three cubically symmetric invariants is written for semiconductors with cubic symmetry of the crystal lattice with an inversion center. The effects of odd linear and cubic in k_{α} terms, which are allowed if the inversion center is lacking, for example, in the T_d point group corresponding to a zinc-blende crystal lattice, are not discussed in this work. It can be easily shown by analogy to Ref. [26], where it was done for electrons from conduction band, that in potentials with inversion symmetry the linear and cubic in wave vector terms in Hamiltonian do not contribute in the first order to hole effective g factor. The linear and cubic in wave vector terms in studied structures do not contribute also in first order to hole spin splitting in zero magnetic field.

The external magnetic field gives two contributions to the hole Hamiltonian (1). The first one is the Zeeman contribution, \widehat{H}_Z [12,27]:

$$\widehat{H}_Z = -2\mu_B \varkappa (\mathbf{J}\mathbf{B}) - 2\mu_B q (J_x^3 B_x + J_y^3 B_y + J_z^3 B_z), \quad (3)$$

with \varkappa and q being magnetic Luttinger parameters [12]. The first term in (3) $\propto \varkappa$ is spherically symmetric and the value of the parameter \varkappa can be estimated by perturbation theory using results of Refs. [8,28] as

$$\varkappa \approx -2/3 + (2\gamma_2 + 3\gamma_3)/3 - \gamma_1/3. \quad (4)$$

The second term in (3) $\propto q$ has cubic symmetry, with axes naturally coinciding with the crystal lattice axes. It is often neglected as the value of q is small in typical semiconductors being two orders of magnitude less than \varkappa [22,27]. The matrix form of \widehat{H}_Z (3), calculated in the standard basis of the topmost Γ_8 valence subband [29,30] is shown in Appendix A, Eq. (A3).

The second contribution from the magnetic field is the orbital contribution, \widehat{H}_B . It comes from the hole wave vector \mathbf{k} in the Luttinger Hamiltonian \widehat{H}_L (2) being replaced by $\mathbf{k} - \frac{e}{c}\mathbf{A}$, where \mathbf{A} is the vector potential of the electro-magnetic field. We consider an arbitrary directed magnetic field and use the symmetric gauge

$$\mathbf{A} = \frac{1}{2}[\mathbf{B} \times \mathbf{r}] = \frac{1}{2}(B_y z - B_z y, B_z x - B_x z, B_x y - B_y x). \quad (5)$$

The given selection of \mathbf{A} is necessary for studying of the hole g factor anisotropy. This task can not be solved if one considers $\mathbf{B}||z$ and $\mathbf{A} = (0, Bx, 0)$ [11,15,31].

The explicit form of the orbital contribution \widehat{H}_B for the gauge (5), neglecting the quadratic on magnetic field terms is shown in Appendix A, Eqs. (A4) and (A6). Note, that the Luttinger Hamiltonian \widehat{H}_L has cubic symmetry due to

valence band warping, $\gamma_2 \neq \gamma_3$. As a result, the magnetic field orbital contribution \widehat{H}_B also inherits cubic symmetry in the case $\gamma_2 \neq \gamma_3$. Both \widehat{H}_L and \widehat{H}_B can be separated into isotropic and cubically symmetric parts, see Eqs. (A1), (A2), (A4), and (A6).

In a weak magnetic field, the effect of the magnetic field on hole states can be calculated using first order perturbation theory by considering \widehat{H}_Z and \widehat{H}_B as perturbations. In the framework of the four-band Luttinger Hamiltonian (2) neglecting the admixing of hole states from spin-orbit split-off valence subband, hole effective g factors would not depend on an NC size, but only on its shape and the type of confining potential [11,15]. As the value of the hole effective g factor is very sensitive to the wave function structure, one first has to find proper zero field wave functions for the zero-filed Hamiltonian $\widehat{H}_L + V_{\text{ext}}(r)$. For our calculations, we use numerical methods developed in Refs. [11,15] and evolved here to take into account $\gamma_2 \neq \gamma_3$ and an arbitrary direction of external magnetic field. We also have developed a numerical method for calculation of hole states in spherical NC with boxlike confining potential.

In zero magnetic field, and in bulk semiconductors for $V_{\text{ext}}(\mathbf{r}) \equiv 0$, the hole states at the top of the valence band ($\mathbf{k} = 0$) are fourfold degenerate. The perturbation \widehat{H}_Z lifts this degeneracy completely in a weak external magnetic field. Without accounting for the cubically symmetric contribution ($q = 0$), this splitting is isotropic and equidistant. The four spin states are characterized by the projection of \mathbf{J} on the magnetic field, and the splitting between neighboring states is equal to $2\kappa\mu_B B$. The nonzero cubically symmetric contribution $\propto q \neq 0$ makes the hole Zeeman splitting anisotropic (dependent on the angle between the magnetic field direction and crystallographic axes) and nonequidistant. If the magnetic field is directed along one of the crystal axes denoted as z , the splitting becomes $E_{-3/2} - E_{+3/2} = 3g_{h,3/2}\mu_B B$ and $E_{-1/2} - E_{+1/2} = g_{h,1/2}\mu_B B$, where g factors of heavy ($J_z = \pm 3/2$) and light ($J_z = \pm 1/2$) holes are

$$g_{h,3/2} = 2\kappa + \frac{9}{2}q, \quad g_{h,1/2} = 2\kappa + \frac{1}{2}q. \quad (6)$$

Note that values of $g_{h,3/2}$ and $g_{h,1/2}$ are different, although this difference is small due to a small value of q [22]. In bulk semiconductors, the contribution \widehat{H}_B becomes important at high magnetic fields, when hole Landau levels are formed [12]. In weak magnetic fields, \widehat{H}_B does not affect the hole g factor.

The situation changes for localized holes, both in zero and external magnetic fields. The symmetry of the localized hole states depends additionally on the symmetry of the external confining potential $V_{\text{ext}}(\mathbf{r})$, which can, in general, be arbitrary. In this work, we consider $V_{\text{ext}}(\mathbf{r})$ with the spherical or cubic symmetry. In the case of a cubically symmetric V_{ext} , it is assumed that the cubic axes of the confining potential coincide with the crystal lattice axes. As a result, the symmetry of the whole system is spherical or cubic.

In spherically symmetric systems, when cubically symmetric corrections can be neglected, the hole states are classified by their total angular momentum $\mathbf{j} = \mathbf{J} + \mathbf{l}$ (\mathbf{l} is the orbital angular momentum) and its projection $j_z = M$ on some marked out axis [25,32]. Due to inversion symmetry, the states with even and odd values of l are separated and the ground states

is in most cases even. In cubic crystals, hole states have to be classified by irreducible representations of the corresponding point group, in our case O_h . Therefore, both the internal angular momentum and the total angular momentum of the hole, as well as their projections, are no longer good quantum numbers [33]. However, the hole ground state in zero magnetic field remains fourfold degenerate and can be traced to the spherically symmetric state with total angular momentum $j = 3/2$. It can be described by cubic invariants constructed from the pseudovector components $j_\alpha = J_\alpha + l_\alpha$ ($\alpha = x, z, y$) transforming like J_α according to the Γ_8 representation. Pseudospin \mathbf{j} can be considered as a generalized hole angular momentum. As we neglect the odd in wave vector contributions to the hole Hamiltonian, all results presented below are valid both for O_h and T_d point groups, so for brevity, we omit the parity indices. We further consider even hole states with $j = 3/2$ and projections $M = j_z = \pm 3/2, \pm 1/2$ on the crystallographic axis z . Importantly, for this state, the matrices j_α in the basis of the eigenstates Ψ_M of the zero-field Hamiltonian $\widehat{H}_L + V_{\text{ext}}$ have the same form as the matrices J_α in the basis of four Bloch functions $u_\mu, \mu = \pm 3/2, \pm 1/2$ of Γ_8 valence band with $J_z = \mu$ [34].

For $V_{\text{ext}}(\mathbf{r}) \neq 0$ the orbital contribution from the magnetic field, \widehat{H}_B , becomes nonzero. In contrast to bulk, for a localized hole two more factors may result in the cubically symmetric corrections to the Zeeman splitting: the cubic shape of the NC coming from $V_{\text{ext}}(\mathbf{r}) \neq 0$ itself, and valence band warping. Both these factors lead to a hole wave function of cubic symmetry in zero magnetic field. We study the effect of these factors in addition to the $\propto q$ cubic term in the Zeeman splitting of the hole states in an external magnetic field.

In an external magnetic field, the effective Zeeman Hamiltonian of a localized hole with $j = 3/2$ can be written as [13]

$$\begin{aligned} \widehat{H}_Z^{\text{eff}} &= -\boldsymbol{\mu}^{\text{eff}} \mathbf{B} \\ &= -\mu_B g_h (\mathbf{j} \mathbf{B}) - 2\mu_B Q^{\text{eff}} (j_x^3 B_x + j_y^3 B_y + j_z^3 B_z), \end{aligned} \quad (7)$$

where g_h and Q^{eff} are responsible for the isotropic and cubically symmetric parts of the hole effective magnetic moment $\boldsymbol{\mu}^{\text{eff}}$, correspondingly. In the general case, $\boldsymbol{\mu}^{\text{eff}}$ is not co-linear to \mathbf{j} and their relation is

$$\boldsymbol{\mu}_\alpha^{\text{eff}} = \mu_B g_h j_\alpha + 2\mu_B Q^{\text{eff}} j_\alpha^3. \quad (8)$$

The first term linear in j in (8) should be written with the help of a second rank tensor as $g_{\beta\alpha}^h j_\beta$, and the second one, cubic in j , with the help of a fourth rank tensor $Q_{\beta\gamma\delta\alpha} j_\beta j_\gamma j_\delta$. In O_h and T_d symmetry, a second rank tensor is diagonal and described by one scalar $g_h^{\text{sph}} = g_{xx}^h = g_{yy}^h = g_{zz}^h$, while the fourth rank tensor $Q_{\beta\gamma\delta\alpha}$ is described by two nonzero constants $Q_1 = Q_{\alpha\alpha\alpha\alpha}^{\text{eff}}$, $\alpha = x, y, z$ and $Q_2 = Q_{\alpha\alpha\beta\beta}^{\text{eff}} = Q_{\alpha\beta\beta\alpha}^{\text{eff}} = Q_{\alpha\beta\alpha\beta}^{\text{eff}}$ with $\alpha \neq \beta$, $\alpha, \beta = x, y, z$. However, as the $j_x^2 + j_y^2 + j_z^2$ transforms as a scalar in O_h and T_d , the two cubically symmetric contributions can be reduced to one isotropic contribution $\propto Q_2$ added to the g_h^{sph} term and one cubically symmetric contribution, so that

$$g_h = g_h^{\text{sph}} + 41Q_2/2, \quad Q^{\text{eff}} = Q_1 - 3Q_2. \quad (9)$$

Deriving Eqs. (8) and (9), we took into account $j_x^2 + j_y^2 + j_z^2 = j(j+1) = 15/4$ for $j = 3/2$ and computational

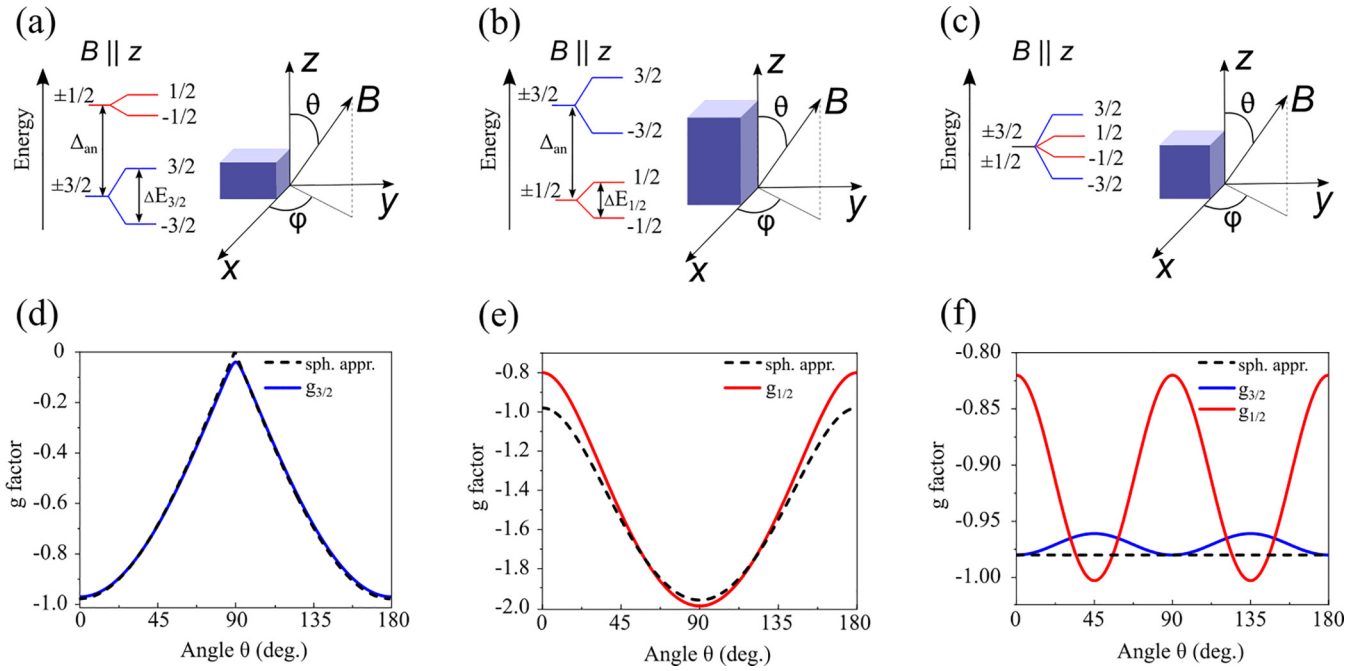


FIG. 1. Schematic of the relative orientation of a NC, applied magnetic field B , and the laboratory frame xyz for an oblate NC (a), prolate NC (b), and cube-shaped NC (c). The schematic shows the splitting of hole states in the presence of uniaxial anisotropy Δ_{an} and applied magnetic field for the shown NC shapes; [(d)–(f)] dependencies of the effective g factors $g_{3/2} = \Delta E_{3/2}/3\mu_B B$ and $g_{1/2} = \Delta E_{1/2}/\mu_B B$ of the hole ground state on the angle θ between magnetic field direction and z . Calculations are done for $\varphi = 0$, $g_h = -0.8$, and $Q^{\text{eff}} = -0.04$. Dashed line corresponds to $g_h = g_h^{\text{sph}} = -0.98$ and $Q^{\text{eff}} = 0$.

relations for $j_\beta j_\gamma - j_\gamma j_\beta = ie_{\beta\gamma\delta} j_\delta$, where $e_{\beta\gamma\delta}$ is a third rank antisymmetric unit tensor.

If the symmetry of V_{ext} is additionally lowered to include some uniaxial perturbation $V_{\text{ext}}^{\text{an}}$ along crystal axis z with corresponding point symmetry group D_{4h} , the hole states with $|M| = 3/2$ (heavy holes) and $|M| = 1/2$ (light holes) are split in zero magnetic field, as shown in Figs. 1(a) and 1(b). Then, the axes z and x, y become nonequivalent, and the hole effective Hamiltonian in an external magnetic field should be written as

$$\hat{H}_Z^{\text{eff}} = -\mu_B [g_\perp (j_x B_x + j_y B_y) + g_\parallel j_z B_z] - 2\mu_B [Q_\perp^{\text{eff}} (j_x^3 B_x + j_y^3 B_y) + Q_\parallel^{\text{eff}} j_z^3 B_z]. \quad (10)$$

Instead of four parameters g_\perp , g_\parallel , Q_\perp^{eff} , and Q_\parallel^{eff} , it is instructive to introduce the following four parameters

$$\begin{aligned} g_{3/2}^\parallel &= g_\parallel + \frac{9}{2} Q_\parallel^{\text{eff}}, & g_{1/2}^\parallel &= g_\parallel + \frac{1}{2} Q_\parallel^{\text{eff}}, \\ g_{3/2}^\perp &= Q_\perp^{\text{eff}}, & g_{1/2}^\perp &= 2g_\perp + 10Q_\perp^{\text{eff}}. \end{aligned} \quad (11)$$

If the splitting energy Δ_{an} between the heavy ($|M| = 3/2$) and light ($|M| = 1/2$) hole states is large as compared with the magnetic field induced splitting, $\Delta_{an} \gg \mu_B B$, in the magnetic field they can be considered separately. In this case, parameters of (11) have the meaning of the effective longitudinal (transverse) g factors describing the splitting of heavy and light hole states in a magnetic field directed parallel (perpendicular) to the anisotropy axis. For an arbitrary field direction, the Zeeman splitting of heavy and light holes, in this case, would be described by the matrices Eq. (A9) given in Appendix A. It is isotropic in xy plane and highly anisotropic

with respect to the angle θ between the magnetic field and z axis:

$$\Delta E_{|M|} = 2|M|\mu_B \sqrt{(g_{|M|}^\parallel B_z)^2 + (g_{|M|}^\perp B_\perp)^2}. \quad (12)$$

where $B_\perp = \sqrt{B_x^2 + B_y^2} = B \sin \theta$.

Importantly, for $B_z = 0$, the Zeeman splitting of holes with $|M| = 3/2$ is not zero only due to a nonzero $g_{3/2}^\perp = Q_\perp^{\text{eff}}$, while the difference between $g_{3/2}^\parallel$ and $g_{1/2}^\parallel$ arises only due to a nonzero Q_\parallel^{eff} . If the cubically symmetric terms are absent in the Luttinger Hamiltonian and external potential, $Q_\perp^{\text{eff}} = 0$, the transverse heavy hole g factor vanishes. At the same time, the uniaxial symmetry of $V_{\text{ext}}^{\text{an}}$, for example, for spheroidal NCs, contributes to $g_\perp \neq g_\parallel \neq g_h^{\text{sph}}$ and induce $Q_\parallel^{\text{eff}} \neq 0$. This results in $g_{3/2}^\parallel \neq g_{1/2}^\parallel$ in spheroidal NCs, as shown in [11].

As we study NCs with shape close to spherical or cubic in what follows, we focus on effects stemming from a nonzero cubically symmetric contribution to the effective Zeeman Hamiltonian (7). We neglect the effect of $V_{\text{ext}}^{\text{an}}$ on the uniaxial anisotropy of hole Zeeman splitting and assume in Eqs. (10) and (11) that

$$g_\perp \equiv g_\parallel \equiv g_h, \quad Q_\perp^{\text{eff}} \equiv Q_\parallel^{\text{eff}} \equiv Q^{\text{eff}}. \quad (13)$$

The effective g factors dependencies on the angle θ , for hole states with $|M| = 3/2$ and $|M| = 1/2$, calculated accounting for the cubic symmetry of the crystal lattice for parameters of CdSe, $g_h = -0.8$ and $Q^{\text{eff}} = -0.04$ are shown in Figs. 1(d) and 1(e), respectively. Dashed lines in Figs. 1(d) and 1(e)

show the effective g factor calculated neglecting lattice symmetry with $g_h = -0.98$ and $Q^{\text{eff}} = 0$.

If the hole states with $|M| = 3/2$ and $|M| = 1/2$ are degenerate in zero magnetic field, the matrix form of the effective Zeeman Hamiltonian is given in Eq. (A8), Appendix A. In this case, a simple expression like Eq. (12) for the hole Zeeman splitting in an arbitrary directed magnetic field cannot be written. For the magnetic field directed along a crystal axis, the four hole states in the magnetic field are characterized by the projection $M_B = \pm 3/2, \pm 1/2$ of \mathbf{j} on \mathbf{B} , $M_B = M$ if $\mathbf{B} \parallel z$. For an arbitrary field direction, the $\propto Q^{\text{eff}}$ term mixes the states with different $M_B = (\mathbf{j}\mathbf{B})/B$ as well as with different $M = j_z$. However, we continue to notate the four eigenstates and their respective Zeeman splitting obtained by the diagonalization of the matrix Eq. (A3) with $M_B = \pm 3/2, \pm 1/2$ and

$$\Delta E_{3/2} = \frac{3}{2}g_{3/2}\mu_B B, \quad \Delta E_{1/2} = \frac{1}{2}g_{1/2}\mu_B B.$$

In that case, the hole Zeeman splittings are anisotropic with all cubic axes being equal. In Fig. 1(f), we show dependence of the effective g factor on the angle θ with the same set of parameters as in Figs. 1(d) and 1(e).

As stated above, the hole Hamiltonian (1) contains three sources of the cubically symmetric contribution to the hole g factor: a crystallographic contribution to the Zeeman Hamiltonian $\propto q$, the shape of the NC coming in form of $V_{\text{ext}}(\mathbf{r})$, and valence band warping, $\gamma_2 \neq \gamma_3$. Below we show how these three factors contribute to g_h and Q^{eff} . It is important to note that the values of g_h and Q^{eff} can be determined from calculations performed for the magnetic field along one of the cubic axes, as they are equal. However, we verify the resulting g factors and Zeeman splittings by direct numeric calculations for an arbitrary direction of magnetic field.

We start from the first two effects and consider in Secs. III A and III B the Hamiltonian (2) in the spherical approximation neglecting valence band warping:

$$\hat{H}_L = \frac{\hbar^2}{2m_0} \left[\left(\gamma_1 + \frac{5}{2}\gamma \right) k^2 - 2\gamma \{J_\alpha J_\beta\} \{k_\alpha k_\beta\} \right], \quad (14)$$

where $\gamma = (2\gamma_2 + 3\gamma_3)/5$ and the bulk light-hole and heavy-hole effective masses are: $m_{lh} = m_0/(\gamma_1 + 2\gamma)$ and $m_{hh} = m_0/(\gamma_1 - 2\gamma)$, respectively. In Sec. III C we consider additionally the effect of the $\gamma_2 \neq \gamma_3$. We demonstrate that the Zeeman crystallographic cubically symmetric contribution $\propto q$ contributes only to the Q_1 constant and, thus, to Q^{eff} , but does not change the isotropic part of hole effective g factor. The cubic shape of NCs as well as the cubic terms in the hole kinetic energy, on the contrary, contribute to both Q_1 and Q_2 , hereby changing isotropic part of hole g factor, g_h , as well as inducing the Q^{eff} term even for $q = 0$.

III. RESULTS AND DISCUSSION

A. Spherically symmetric nanocrystals

For spherically symmetric NCs considered in the spherical approximation of the Luttinger Hamiltonian (14), the cubically symmetric contribution to the hole g factor may originate only from the term $\propto q$ in \hat{H}_Z . In a spherically symmetric external potential $V_{\text{ext}}(\mathbf{r})$ with isotropic kinetic energy, hole states can be classified by their total angular momentum j

[25,32,35,36] and their wave functions are [25]

$$\Psi_{jM} = \sqrt{2j+1} \sum_l (-1)^{l-3/2+M} (i)^l R_{jl}(r) \times \sum_{m+\mu=M} \begin{pmatrix} l & 3/2 & j \\ m & \mu & -M \end{pmatrix} Y_{l,m} u_\mu. \quad (15)$$

Here, Y_{lm} are spherical harmonics [37] being the eigenfunctions of the hole orbital momentum l , $\begin{pmatrix} l & k & l \\ m & n & p \end{pmatrix}$ are $3j$ Wigner symbols. The ground hole state is a fourfold degenerate SD -like state and consists of functions with $l = 0$ and $l = 2$. For simplicity, we denote the respective radial functions as $R_0(r)$ and $R_2(r)$.

For $q = 0$, the hole g factor was calculated in Ref. [14] and can be written as (see Eq. (12) of Ref. [11] in the limit of strong spin-orbit interaction)

$$g_h^{\text{sp}} = 2\kappa S(\beta) + \frac{4}{5}\gamma_1 I(\beta),$$

$$S(\beta) = \left(1 - \frac{4}{5}I_2^g\right), \quad I(\beta) = \frac{1-\beta}{1+\beta}I_1^g + \frac{2\beta}{1+\beta}I_2^g, \quad (16)$$

where β is the light to heavy hole effective mass ratio $\beta = (\gamma_1 - 2\gamma)/(\gamma_1 + 2\gamma)$. Function $S(\beta)$ describes the renormalization of the isotropic part of the Zeeman contribution \hat{H}_Z , function $I(\beta)$ describes the orbital contribution to the g factor stemming from \hat{H}_B . Integrals I_1^g and I_2^g were introduced in Ref. [14]:

$$I_1^g = \int_0^\infty r^3 R_2(r) \frac{dR_0(r)}{dr} dr, \quad I_2^g = \int_0^\infty r^2 R_2^2(r) dr. \quad (17)$$

The dependencies $I(\beta)$ and $S(\beta)$ for a spherically symmetric NC with parabolic and boxlike potentials are shown in Fig. 2.

If $q \neq 0$, the corresponding contribution to the hole g factor can be calculated using first order perturbation theory. It can be easily shown, that for a hole wave function in the form of Eq. (15), $Q_2 = 0$, $g_h = g_h^{\text{sp}}$ and $Q^{\text{eff}} = Q_1 = Q^q$, where function $Q^q(\beta)$ can be written as

$$Q^q(\beta) = \left(1 - \frac{4}{5}I_2^g\right) = S(\beta). \quad (18)$$

One can see in Fig. 2 that $Q^q(\beta) = S(\beta)$ does not exceed unity in the whole range of β . Thus, in spherical NCs, the contribution to the hole g factor from the cubically symmetric part of the Zeeman Hamiltonian is comparable to the corresponding contribution in bulk.

B. Cube-shaped nanocrystals

In cube-shaped NCs there is an additional source of the cubic symmetry arising from the shape of the NC. As an example, we consider cube-shaped NCs with a rectangular infinite confining potential. It was shown that the hole ground state is an even S -like state for the majority values of β , although, for $0.1425 \gtrsim \beta \gtrsim 0.0775$ the ground state for cube-shaped NCs with boxlike infinite potential is a P -like odd state [11]. Both states are fourfold degenerate, as the cubically symmetric terms in the Luttinger Hamiltonian do not split states with total angular momentum less than $5/2$ [33]. Here we consider only the lowest even hole state, which can be traced to the $S_{3/2}$ state in spherical NCs.

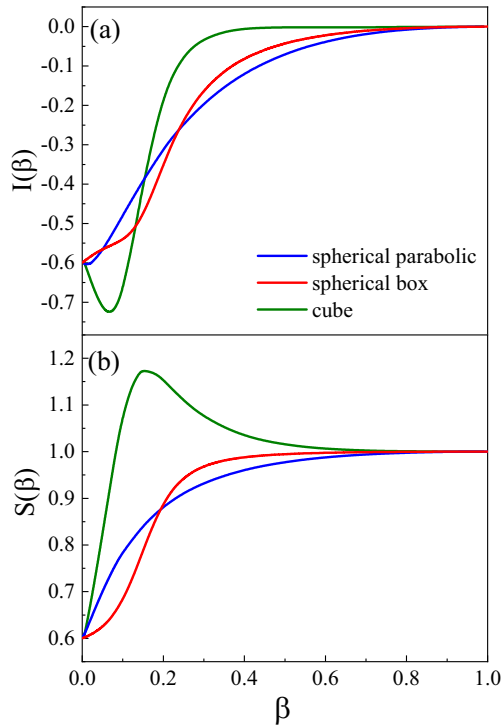


FIG. 2. Dependencies of the functions (a) $I(\beta)$ and (b) $S(\beta)$ on the light to heavy hole effective mass ratio β for spherical NCs with parabolic and boxlike potentials and cube-shaped NCs.

As we have shown in Ref. [11], even if we neglect the cubic contribution to the Zeeman Hamiltonian (3), and consider the Luttinger Hamiltonian in the spherical approximation, g factors of “heavy” ($|j_z| = 3/2$) and “light” ($|j_z| = 1/2$) holes are different in cube-shaped NCs. In Ref. [11] we qualitatively explained this result by an effective cubically symmetric contribution to the hole g factor coming from the NC shape. In this work, we study the effect of the cubic shape of the NC in more detail.

Unlike the wave functions of the hole confined in a spherical NC, those for a cube-shaped NC can not be written in a simple analytical form. We find the hole energy spectrum and wave functions numerically using our previously developed method (see Ref. [11]). The wave functions are found as the expansion on the basis of hole eigenfunctions in the parabolic band model in the same NC. Then the matrix elements for the kinetic energy, as well as the magnetic field contributions, are found and the eigenstates and eigenenergies are obtained by diagonalizing the resulting matrix-form Hamiltonian. Here, we also expand our method for an arbitrary oriented magnetic field.

The cubic shape of the NC leads to additional contributions to g_h and Q^{eff} as compared with spherical NCs, Eqs. (16) and (18). Phenomenologically, one can write

$$g_h = I(\beta)\gamma_1 + 2S(\beta)\varkappa + G^q(\beta)q, \quad (19)$$

$$Q^{\text{eff}} = Q^y(\beta)\gamma_1 + Q^z(\beta)\varkappa + Q^q(\beta)q. \quad (20)$$

Here, functions $I(\beta)$, $S(\beta)$, $G^q(\beta)$, $Q^y(\beta)$, $Q^z(\beta)$, and $Q^q(\beta)$ depend only on the light to heavy hole effective mass ratio β , and on the type and shape of the NC potential. Function

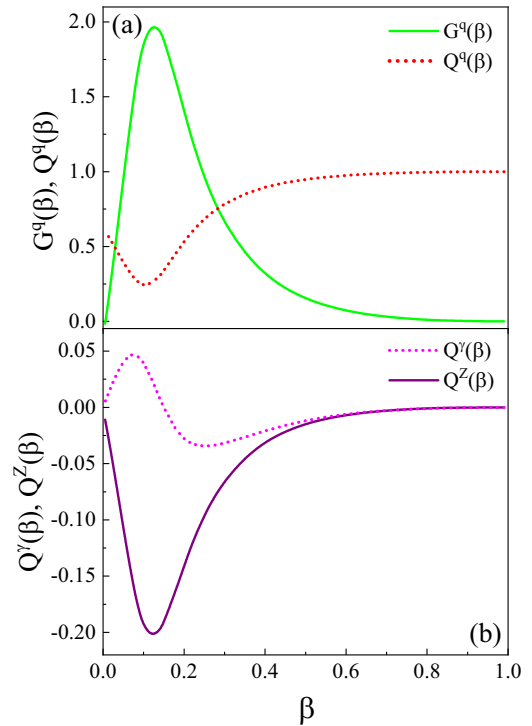


FIG. 3. Dependencies of functions (a) $G^q(\beta)$ and $Q^q(\beta)$; (b) $Q^y(\beta)$ and $Q^z(\beta)$ on the light to heavy hole effective mass ratio β for cube-shaped NCs, calculated numerically.

$G^q(\beta) \propto Q_2$ describes the contribution of the cubically symmetric term in the Zeeman Hamiltonian (3) to the isotropic part of the effective Zeeman Hamiltonian (7). Importantly, here $Q_2 \neq 0$ only due to the cubic symmetry of the hole wave functions inside a NC. In addition, the cubic symmetry of the wave functions induces two absent in spherical NCs contributions into Q^{eff} term proportional to the parameters of the isotropic Luttinger Hamiltonian and described by the functions $Q^y(\beta)$ and $Q^z(\beta)$. Expressions (19) and (20) are reduced to Eqs. (16) and (18) for spherical NCs, if one take $G^q(\beta) \equiv Q^y(\beta) \equiv Q^z(\beta) \equiv 0$.

For cube-shaped NCs, all functions from Eqs. (19) and (20) are nonzero and have to be calculated numerically. The dependencies $I(\beta)$ and $S(\beta)$ are shown in Fig. 2, $G^q(\beta)$, $Q^q(\beta)$, $Q^y(\beta)$, $Q^z(\beta)$ are shown in Fig. 3. Interestingly, for cube-shaped NCs, unlike spherical ones, $Q^q(\beta) \neq S(\beta)$. This fact is the consequence of difference between the structure of hole wave function in spherical and cube-shaped NCs. From Fig. 3(b), one can see that in cube-shaped NCs contributions to Q^{eff} from the orbital magnetic field contribution \hat{H}_B and from the isotropic part of the Zeeman Hamiltonian can be quite large for typical $\beta \approx 0.2$ in the semiconductors we are interested in (see Table I). It results in substantial hole Zeeman splitting anisotropy, even in the absence of valence band warping. The parameter $Q^q(\beta)$ in cube-shaped NCs, as in spherical NCs, is less than unity and leads to only a small contribution from the crystallographic Zeeman Hamiltonian $\propto q$ to Q^{eff} . A larger value of $G^q(\beta)$ also leads to small renormalization of the isotropic g_h part of the hole g factor due to a small value of q .

TABLE I. Valence band parameters used for the calculation of the hole Zeeman splitting.

No.	Material	γ_1	γ_2	γ_3	β	\varkappa	α	q	Refs. ^a
1	zb-CdSe	2.52	0.65	0.95	0.2	-0.12	0.36	—	[43]
2	zb-ZnSe	3.94	1.00	1.52	0.2	0.21	0.4	—	[44]
3	CdTe	4.14	1.09	1.62	0.19	0.3	0.38	—	[45]
4	GaAs	6.79	1.92	2.68	0.18	1.03	0.32	0.017	[22,46]

^aReferences are given for the γ_1 , γ_2 , γ_3 and q Luttinger parameters, and we use relations $\beta = (\gamma_1 - 2\gamma_2)/(\gamma_1 + 2\gamma_2)$ and $\varkappa \approx 2/3 + 5\gamma_3/3 - \gamma_1/3$ with $\gamma = (2\gamma_2 + 3\gamma_3)/5$ and $\alpha = (\gamma_3 - \gamma_2)/\gamma$.

C. The effect of valence band warping

The spherical approximation for the Luttinger Hamiltonian, Eq. (14), is widely used and has proved itself effective in calculating the energy of the hole ground state. This approximation gives a correct hole ground state energy in any spherically symmetric potential in first order perturbation theory, while the second order corrections are also usually small as in typical semiconductors $\gamma_3 - \gamma_2 \ll \gamma_3 + \gamma_2$ [38]. On the other hand, the effect of the valence band warping, $\gamma_2 \neq \gamma_3$, on the hole g factor is expected to be stronger due to nonzero first order corrections to the hole wave functions. Indeed, the renormalization of the hole g factor in nanostructures is controlled to a large extent by the mixing of hole states with different momentum projections on the magnetic field [11]. This mixing is modified strongly by the kinetic energy term $\propto \alpha$, Eq. (A2), with $\alpha = (\gamma_3 - \gamma_2)/\gamma$ being the parameter characterizing valence band warping. This effect is qualitatively similar to the effect of the cubic shape of NCs in the case $\gamma_2 = \gamma_3$, considered in previous section.

Here, we discuss the effect of valence band warping on the hole Zeeman splitting in an external magnetic field. Unlike the cubically symmetric contribution to the Zeeman Hamiltonian (3), valence band warping cannot be taken into account by first order perturbation theory with wave functions from Eq. (15) as good zero order approximation functions. The correct functions must account for valence band warping even in zero magnetic field [39–42], and these functions cannot be found analytically. The full analysis of the effect of valence band warping on the hole effective g factor for arbitrarily β is beyond the scope of this work. Here, we confine ourselves to the numerical analysis of the warping effect in a number of semiconductors.

To obtain the Zeeman splitting of the hole ground state in spherical parabolic potential and cube-shaped NCs, we calculate first hole wave functions in zero magnetic field using our numerical methods developed for spherical approximation of the Luttinger Hamiltonian and modified appropriately to take valence band warping into account [11,31]. As we use the full basis (accurate within its finite size in real calculation), obtained results are valid also when the nonspherical kinetic energy term of the hole Hamiltonian is included. We develop additionally the numerical method for calculating hole wave functions in spherical NCs with boxlike potential accounting for the valence band warping as described in Appendix B. Importantly, even in spherical NCs the account of the valence band warping results into cubical anisotropy of the hole spatial distribution. Then, the Zeeman splitting in magnetic field is found treating $\hat{H}_Z + \hat{H}_B$ as the perturbation, where \hat{H}_B

includes both isotropic and cubically symmetric terms $\propto \alpha$ (see Appendix A).

The valence band warping leads to nonspherical hole constant-energy surfaces in bulk semiconductor. As an example in Fig. 4(a), we show the constant-energy curves of

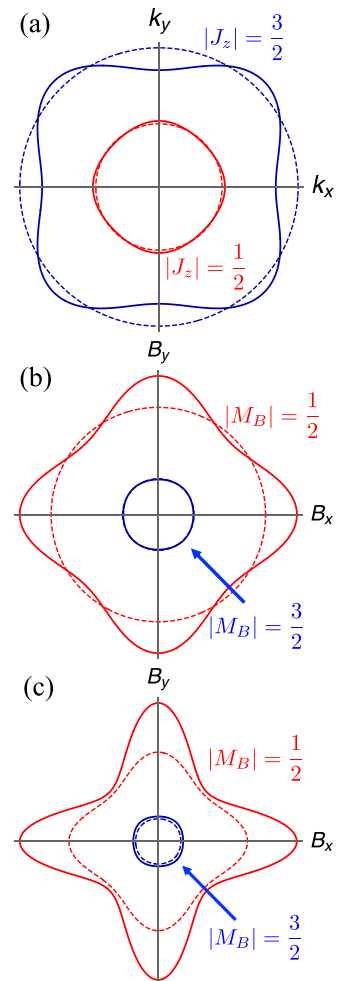


FIG. 4. (a) Constant-energy curves of bulk heavy, $J_z = 3/2$ (blue color), and light holes, $J_z = 1/2$ (red color), in xy plane, (b) and (c) Constant-Zeeman-splitting curves for hole states with $|M_B| = 3/2$ blue color and $|M_B| = 1/2$ red color calculated for spherical and cube-shaped NCs with boxlike potential, correspondingly. Calculations were made for CdSe parameters $\gamma_1 = 2.52$, $\gamma_2 = 0.65$, $\gamma_3 = 0.95$ [43], solid lines correspond to accounting for valence band warping, dashed lines correspond to spherical approximation of the Luttinger Hamiltonian with $\gamma_2 = \gamma_3 = \gamma = 0.83$.

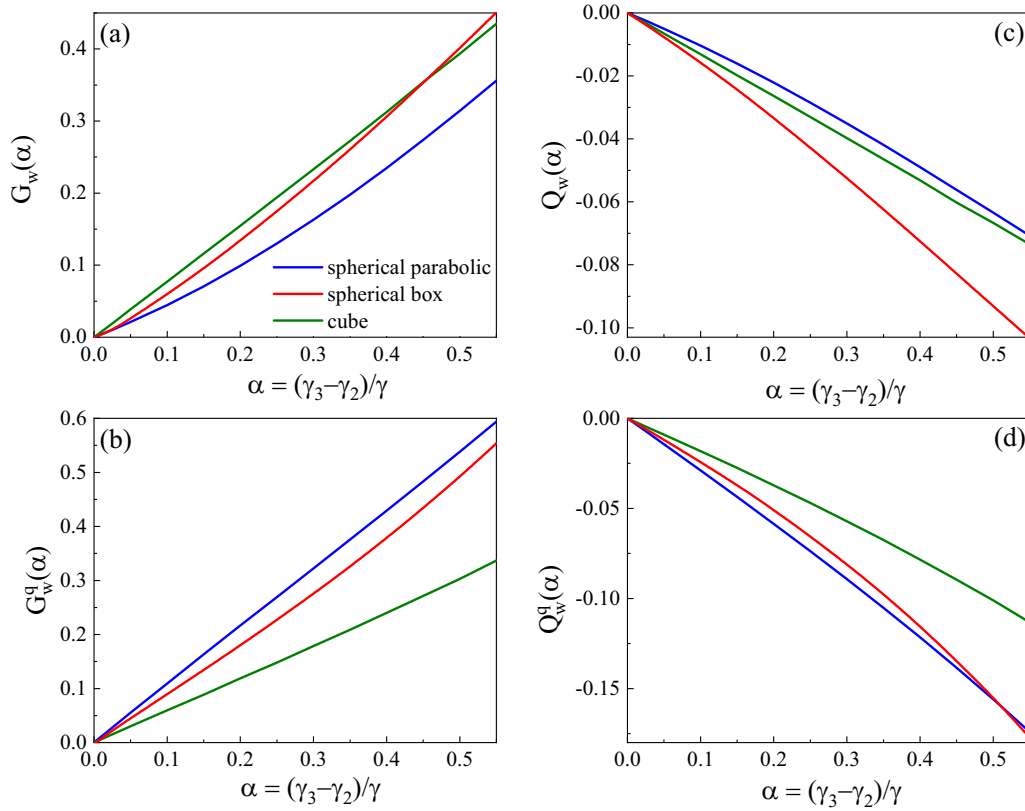


FIG. 5. Functions (a) $G_w(\alpha)$, (b) $G_w^q(\alpha)$, (c) $Q_w(\alpha)$, and (d) $Q_w^q(\alpha)$ calculated numerically for CdSe valence parameters [43].

bulk heavy and light holes in xy plane in zero magnetic field, calculated for CdSe parameters $\gamma_1 = 2.52$, $\gamma_2 = 0.65$, $\gamma_3 = 0.95$ (corresponding to $\gamma = 0.83$) [43], solid lines correspond to accounting for the valence band warping, dashed lines correspond to the spherical approximation of the Luttinger Hamiltonian. In Fig. 4(a), one can clearly see cubic symmetry of constant-energy curves and more pronounced anisotropy for heavy holes if $\gamma_2 \neq \gamma_3$. In Figs. 4(b) and 4(c), we show the constant-Zeeman-splitting curves in external magnetic field $\mathbf{B} = (B_x, B_y, 0)$ for states with $|M_B| = 3/2$ and $|M_B| = 1/2$ calculated for spherical and cube-shaped NCs, respectively, with the same Luttinger parameters. In contrast to the Fig. 4(a), the anisotropy is more pronounced for holes with $|M_B| = 1/2$. Due to the equivalence of all cubic axes, the picture would be the same for any plane containing two cubic axes. It is noteworthy, that in the presence of the uniaxial splitting Δ_{an} of the localized hole states with $|M| = 3/2$ and $1/2$ [see Figs. 1(a) and 1(b)], which allows one to neglect their mixing, the transverse g factor in the plane perpendicular to the anisotropy axis becomes isotropic, even with accounting for valence band warping. The only anisotropy in that case would be with respect to the angle with the z axis (transverse or longitudinal g factor).

Let us proceed to a quantitative analysis of the hole g factor anisotropy. The g factor components g_h (19) and Q^{eff} (20) now also depend on the valence band warping parameter α . For illustrative purposes, we numerically calculated those dependencies with valence band parameters for zinc-blende CdSe: $\gamma_1 = 2.52$, $\gamma = 0.83$ [43], changing γ_2 and γ_3 in such a way, that value of $\gamma = (2\gamma_2 + 3\gamma_3)/5 = 0.83$ and $\beta = 0.2$

remain constant. Simultaneously, the value of $\varkappa = -0.12$, determined from Eq. (4) is also constant. As we are interested now only in dependencies of g_h and Q^{eff} on α , it is convenient to write them as

$$g_h(\alpha) = G_0 + G_w(\alpha) + (G_0^q + G_w^q(\alpha))q, \quad (21)$$

$$Q^{\text{eff}}(\alpha) = Q_0 + Q_w(\alpha) + (Q_0^q + Q_w^q(\alpha))q. \quad (22)$$

Here G_0 , G_0^q , Q_0 , and Q_0^q describe g_h and Q^{eff} calculated after Eqs. (19) and (20) for $\alpha = 0$ and fixed values of β and \varkappa . Accounting for $\alpha \neq 0$ leads to cubically symmetric shape of hole wave function in zero magnetic field, and, consequently, to additional contributions to Q_2 tensor component even in spherical NCs. This results in new contributions to both g_h , described by the functions $G_w(\alpha)$ and $G_w^q(\alpha)$, and Q^{eff} , described by the functions $Q_w(\alpha)$ and $Q_w^q(\alpha)$, respectively.

The numerically calculated dependencies of $G_w(\alpha)$, $G_w^q(\alpha)$, $Q_w(\alpha)$, and $Q_w^q(\alpha)$ for chosen CdSe parameters for spherical NCs with parabolic and boxlike potentials, and cube-shaped NCs are shown in Fig. 5. For $\gamma_2 = 0.65$ and $\gamma_3 = 0.95$ [43] (parametrization “1” in Table I), we get $\alpha \approx 0.36$. Corrections $G_w(\alpha)$ and $Q_w(\alpha)$ are quite large at $\alpha \approx 0.36$, leading to noticeable renormalization of g_h and Q^{eff} due to valence band warping. The dependence of hole g factors on the magnetic field direction in spherical NCs with parabolic confining potentials corresponding to parameters of CdSe, parametrization “1” in Table I, is shown in Fig. 1(f). One can see a strong difference to the spherical approximation for light holes and a rather small difference for heavy holes. In Figs. 1(d) and 1(e), the dependencies of hole g factors on the

TABLE II. Parameters $g_{3/2}^{\parallel}$, $g_{1/2}^{\parallel}$, $g_{3/2}^{\perp}$, $g_{1/2}^{\perp}$, g_h , and Q^{eff} calculated for semiconductor NCs with different shape and type of confining potential, numbers brackets corresponds to spherical approximation of Luttinger Hamiltonian. Material parameters used for calculations are given in Table I.

Spherical NCs with parabolic potential							
No	Material	$g_{3/2}^{\parallel}$	$g_{1/2}^{\parallel}$	$g_{3/2}^{\perp}$	$g_{1/2}^{\perp}$	g_h (g_h^{sph})	Q^{eff}
1	zb-CdSe	-0.97 (-0.98)	-0.8(-0.98)	-0.04(0)	-1.99 (-1.96)	-0.777(-0.98)	-0.04(0)
2	zb-ZnSe	-0.85(-0.86)	-0.49(-0.86)	-0.09(0)	-1.79(-1.72)	-0.444(-0.86)	-0.09(0)
3	CdTe	-0.8(-0.82)	-0.45(-0.82)	-0.09 (0)	-1.7(-1.64)	-0.4(-0.82)	-0.09(0)
4	GaAs, $q = 0$	-0.58 (-0.61)	-0.006 (-0.61)	-0.14 (0)	-1.3 (-1.22)	0.067(-0.61)	-0.14(0)
5	GaAs, $q = 0.017$	-0.52 (-0.61)	0.007 (-0.61)	-0.13 (0)	-1.16 (-1.22)	0.07(-0.61)	-0.13(0)
Spherical NCs with boxlike potential							
No.	Material	$g_{3/2}^{\parallel}$	$g_{1/2}^{\parallel}$	$g_{3/2}^{\perp}$	$g_{1/2}^{\perp}$	g_h (g_h^{sph})	Q^{eff}
1	zb-CdSe	-1.08(-1.06)	-0.82(-1.06)	-0.064 (0)	-2.21 (-2.12)	-0.78 (-1.06)	-0.064 (0)
2	zb-ZnSe	-1.02 (-1)	-0.55 (-1)	-0.12(0)	-2.17 (-2)	-0.5(-1.03)	-0.12(0)
3	CdTe	-1.01 (-1.03)	-0.54 (-1.01)	-0.12 (0)	-2.16 (-2.2)	-0.48(-1.01)	-0.12(0)
4	GaAs, $q = 0$	-1.08 (-1.06)	-0.36 (-1.06)	-0.18(0)	-2.34 (-2.12)	-0.27(-1.06)	-0.18(0)
5	GaAs, $q = 0.017$	-1.05 (-1.06)	-0.355 (-1.06)	-0.173(0)	-2.26 (-2.12)	-0.26(-1.06)	-0.17(0)
Cube-Shaped NCs							
No.	Material	$g_{3/2}^{\parallel}$	$g_{1/2}^{\parallel}$	$g_{3/2}^{\perp}$	$g_{1/2}^{\perp}$	g_h	Q^{eff}
1	zb-CdSe	-0.87 (-0.96)	-0.47 (-0.73)	-0.1 (-0.058)	-1.84 (-1.98)	-0.42(-0.7)	-0.1(-0.058)
2	zb-ZnSe	-0.76 (-0.87)	-0.17 (-0.3)	-0.15 (-0.14)	-1.68 (-1.88)	-0.09(-0.24)	-0.15(-0.14)
3	CdTe	-0.75 (-0.86)	0.24 (-0.26)	-0.25 (-0.15)	-1.76 (-1.86)	0.37(-0.19)	-0.25(-0.148)
4	GaAs, $q = 0$	0.58 (-0.72)	1.3 (0.42)	-0.18(-0.29)	1 (-1.8)	1.4(0.58)	-0.18(-0.295)
5	GaAs, $q = 0.017$	0.5 (-0.72)	1.33 (0.42)	-0.2(-0.29)	0.8 (-1.8)	1.44(0.58)	-0.2(-0.295)

magnetic field direction are shown for the case of split states of heavy and light holes. Here the difference is smaller than in the spherical case.

Parameters $g_{3/2}^{\parallel}$, $g_{1/2}^{\parallel}$, $g_{3/2}^{\perp}$, and $g_{1/2}^{\perp}$ in spherical NCs with parabolic and boxlike infinite potentials and cube-shaped NCs with boxlike infinite potential, calculated for several semiconductors (for parameters see Table I) are shown in Table II. Numbers in brackets correspond to the spherical approximation of the Luttinger Hamiltonian. As we know the value of q only for GaAs, all calculations were made for $q \equiv 0$. Corresponding values of g_h and Q^{eff} are also shown in Table II.

The contribution to Q^{eff} induced by valence band warping is quite substantial and comparable to the contribution from the cubic shape of NC. A similar effect was reported for acceptors [13] and disklike quantum dots [47], where the quite large cubically symmetric contribution to hole Zeeman splitting coming from valence band warping was reported. The mixing of hole states with momentum projections $+3/2$ and $-3/2$ in transvers magnetic field in trigonal quantum dots allowed due to reduction of symmetry to C_{3v} point group had been reported in Refs. [48,49]. Note that depending on semiconductor, contributions to Q^{eff} from cubic shape of NC and valence band warping in cube-shaped NCs could be of the same or opposite signs. As one can see comparing Figs. 4(b) and 4(c), the cubic anisotropy of the light hole Zeeman splitting is pronounced already in spherical NCs made of zb-CdSe and is enhanced by factor of 2 in cube-shaped NCs. Although, corrections to g_h and Q^{eff} are noticeable, for heavy hole they numerically almost compensate each other resulting in much

weaker anisotropy, see corresponding curves in Figs. 4(b) and 4(c).

As mentioned above, we made all our estimations of the effect of valence band warping on hole g factors for $q \equiv 0$ because only the value for GaAs is known from the literature. Here, we demonstrate the smallness of the $q \neq 0$ effect. We made a calculation taking into account $q \neq 0$ for GaAs. The results are also shown in Table II in lines with label 5. One can see a small difference, as compared to lines with label 4, corresponding to the same set of Luttinger parameters and $q = 0$.

IV. POSSIBLE EXPERIMENTAL MANIFESTATIONS OF THE HOLE g FACTOR CUBIC ANISOTROPY

In this section, we discuss possible experimental consequences of the nonzero value of Q^{eff} . Let us firstly discuss manifestations of the hole g factor anisotropy in the case of colloidal nanostructures with split states of light and heavy holes [see Fig. 1(a)], such as spheroidal or cuboidal nanocrystals, where splitting can reach tens of meV, or nanoplatelets with a splitting up to 300 meV [50]. In such structures, the value of the transverse g factor of the heavy hole, $g_{3/2}^{\perp}$, is determined only by the cubically symmetric contribution Q^{eff} to the effective Zeeman Hamiltonian. Due to a large splitting of the light and heavy hole states in these structures, a fast hole spin relaxation, usually observed in bulk semiconductors, should be suppressed. It opens the possibility for detection

of the Q^{eff} related contribution from studies of the hole spin precession, as was done for epitaxial quantum wells [22–24].

Another possible manifestation concerns the degree of circular polarization (DCP) of photoluminescence in a magnetic field for ensembles of neutral colloidal nanocrystals or nanoplatelets. At low temperatures, the photoluminescence properties of these nanostructures are determined by emission of dark excitons with the projection of the total angular momentum of an electron and a hole $F_z = 2$ on the anisotropy axis [16]. It was shown theoretically in Ref. [17] that DCP should reach 75% for an ensemble of randomly oriented NCs in high magnetic fields. However, this upper limit was never observed experimentally. It was proposed previously that a low saturation value of DCP is caused by nonradiative recombination of dark excitons [17], or by linearly polarized phonon-assisted emission of dark excitons [51].

Our analysis shows that a nonzero transverse g factor of the heavy hole, $g_{3/2}^{\perp} \propto Q^{\text{eff}}$, also can affect the saturation value of DCP. In Ref. [17], it was assumed that dark exciton states with $F_z = \pm 2$ gain oscillator strength in a transverse magnetic field due to mixing of electron spin states $\pm 1/2$. Under this condition, the bright exciton state with $F_z = +1(-1)$ admixes to the state $F_z = +2(-2)$, respectively. The dark exciton states $F_z = \pm 2$ inherit optical properties of the bright exciton states and emit σ^{\pm} polarized light along the anisotropy axis of a nanocrystal, respectively [see Fig. 6(a)]. The nonzero component $g_{3/2}^{\perp}$ allows admixture of the bright exciton state $F_z = +1(-1)$ to the dark exciton state $F_z = -2(+2)$. It results in opposite circular polarization of photons emitted by the dark exciton states and in a decrease of the DCP saturation value. The decreasing factor depends on the angle θ between the anisotropy axis of a NC and magnetic field direction. For a given angle θ , this factor equals $(a_{-1}^2 - a_{+1}^2)/(a_{-1}^2 + a_{+1}^2)$, where $a_{+1/-1}$ are amplitudes of the $F_z = \pm 1$ exciton states in the wavefunction of the $F_z = -2$ dark exciton state, which is usually the lowest in energy (i.e. predominantly populated) exciton state. Amplitudes a_{-1} and a_{+1} are proportional to electron g factor, g_e , and parameter Q^{eff} , respectively. It means that depending on the ratio g_e/Q^{eff} , the value of the dark exciton DCP can vary in a wide range.

Now, let us consider cube-shaped NCs, where a large anisotropy of the hole g factor is expected. In these NCs, the ground hole state is fourfold degenerate in the absence of a magnetic field. Thus one cannot expect experimental observation of Q^{eff} related effects using time-resolved spectroscopy due to a fast hole spin decoherence. We suppose that observation of these effects can be realised by photoluminescence spectroscopy of single cube-shaped NCs in an applied magnetic field. For this purpose, the best candidate is the negatively charged trion (a hole plus two electrons in a singlet state), since its spin splitting is determined solely by the hole g factor and there is no exchange interaction due to the singlet electrons configuration.

In our considerations, we assume that a cube-shaped NC stands on a substrate, and its edges are directed along the axes of the laboratory coordinate system, as shown in Fig. 1(c). A magnetic field is applied in the xz plane at an arbitrary angle θ . The photoluminescence signal is determined by photons emitted along the z axis. The excited state of the system is the

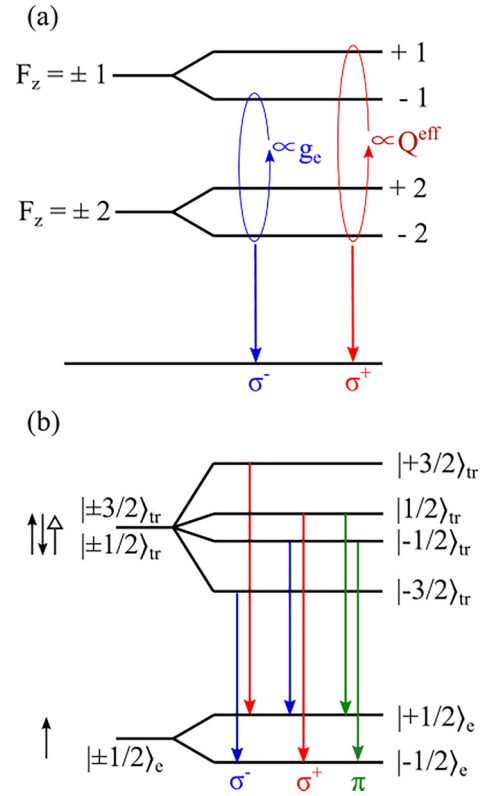


FIG. 6. (a) Schematic of the Zeeman splitting of the dark $F_z = \pm 2$ and bright $F_z = \pm 1$ exciton states in NCs with a large anisotropic splitting Δ_{an} . Arrows show admixture of bright exciton states to the lowest dark state $F_z = -2$ resulting in its emission with σ^+ or σ^- polarization. (b) Optical transitions for a negatively charged trion with magnetic field applied at angle $\theta = 0$ with respect to the crystal z axis. Blue, red, and green arrows show transitions with σ^- , σ^+ , and π polarization, respectively. Black and white arrows show spin of the electron and hole, respectively.

negative trion. Its spin splitting in an applied magnetic field is determined by the spin splitting of hole spin states. After the radiative recombination of the trion, there remains one electron with the spin projection up or down in the magnetic field direction. For a tilted magnetic field, the excited and ground eigenstates of the system are superpositions of the hole and electron basis states along the z axis, respectively. It results in an angular dependence of the energy and oscillator strength of trion emission lines. A schematic of the energy states of the system and possible allowed transition for magnetic field directed in the Faraday geometry (along the z axis of the laboratory frame) is shown in Fig. 6(b). Details of the calculation can be found in Appendix C.

We performed calculations for cube-shaped NCs made of CdSe, CdTe, GaAs and ZnSe with edge size of 15 nm, according to a typical size from [3]. In our model, the only size-dependent parameter is the electron g factor. Its size dependence can be found within the $\mathbf{k} \cdot \mathbf{p}$ method [11]. For the NC size of 15 nm, the calculated electron g factor equals: $g_e(\text{CdSe}) = 0.5$, $g_e(\text{CdTe}) = -1$, $g_e(\text{GaAs}) = 0.3$, and $g_e(\text{ZnSe}) = 1.2$. The upper row in Fig. 7 corresponds to the spherical approximation of the Luttinger

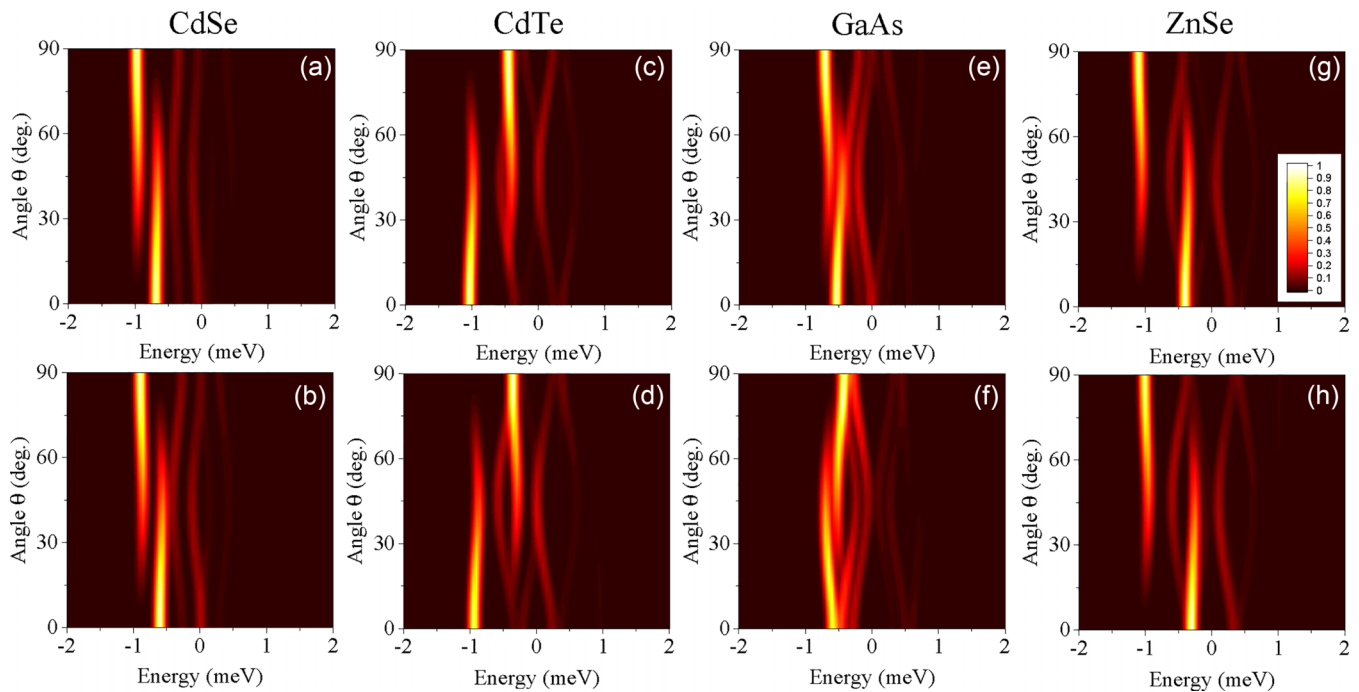


FIG. 7. Calculated spectra of the negative trion at $T = 4$ K and $B = 10$ T in cube-shaped NCs of 15 nm size for [(a) and (b)] CdSe, [(c) and (d)] CdTe, [(e) and (f)] GaAs, and [(g) and (h)] ZnSe. The upper row is calculated for the spherical approximation of the Luttinger Hamiltonian with $\gamma_2 = \gamma_3$. The bottom row is calculated for the full Luttinger Hamiltonian with $\gamma_2 \neq \gamma_3$.

Hamiltonian with $\gamma_2 = \gamma_3$. The bottom row in Fig. 7 corresponds to the full Luttinger Hamiltonian with $\gamma_2 \neq \gamma_3$. One can see that even in the spherical approximation of the Luttinger Hamiltonian, the NC cubic shape affects the angular dependence of the energies of the trion emission lines. Accounting for valence band warping changes the values of the trion lines splitting but does not strongly modify their angular dependencies. We note, that in the absence of valence band warping and the NC cubic shape, the energies of the trion emission lines do not depend on the direction of the applied magnetic field. Thus experimental observation of the angular dependencies shown in Fig. 7 should give evidence of the hole g factor anisotropy.

It is worth noting that the cubic symmetry contribution to the Zeeman splitting cannot arise in perovskites or CuCl nanocrystals even of cubic shape. In these materials, the conduction and valence bands are characterized by a total angular momentum j of electron or hole equal to $1/2$. In perovskites, the anisotropy of charge carriers g factors appears only if the symmetry of the structure, of crystal lattice or of NCs shape is lower than cubic [52]. Experimental techniques, suitable for observation nonequidistant hole spin-splitting of the hole bound to acceptor were discussed in Ref. [53].

V. CONCLUSION

We demonstrated that the Zeeman splitting of hole states inherits both the shape and lattice symmetry of nanocrystals made of zinc-blende semiconductors. We show that the cubic shape of a nanocrystal and cubic symmetry of the

zinc-blende crystal lattice make comparable contributions to the hole Zeeman splitting. In both cases, effects arise due to the cubically symmetric instead of spherically symmetric spatial distribution of the hole wave functions and, consequently, renormalized light hole to heavy hole mixing. The resulting hole Zeeman splitting is nonequidistant and depends on the direction of the magnetic field with respect to the cubic axes. We show that both cubically symmetric contributions are large enough and should be taken into account in analysis of magneto-optical studies of spin splitting of hole states. Possible experimental manifestations of the predicted cubic anisotropy of hole Zeeman splitting in semiconductor nanocrystals are discussed.

ACKNOWLEDGMENTS

We thank D.R. Yakovlev for valuable discussions. This work was funded by the Russian Science Foundation (Grant No. 23-12-00300) [54].

APPENDIX A: MATRIX FORM OF HOLE HAMILTONIANS

We present the Luttinger Hamiltonian describing hole kinetic energy in two terms: $H_L = H_L^{\text{sph}} + \alpha H_L^\alpha$, where the first one represents the spherically symmetric part and the second describes the valence band warping with its characterizing parameter $\alpha = (\gamma_2 - \gamma_3)/\gamma$. In the standard basis of the topmost Γ_8 valence subband u_μ ($\mu = +3/2, +1/2, -1/2, -3/2$)

[29,30] Hamiltonians H_L^{sph} and H_L^α in matrix form are

$$\hat{H}_L^{\text{sph}} = \frac{\hbar^2}{2m_0} \begin{pmatrix} P+Q & H & I & 0 \\ H^\dagger & P-Q & 0 & I \\ I^\dagger & 0 & P-Q & -H \\ 0 & I^\dagger & -H^\dagger & P+Q \end{pmatrix}, \quad P = \gamma_1(k_x^2 + k_y^2 + k_z^2), \quad Q = \gamma(k_x^2 + k_y^2 - 2k_z^2),$$

$$H = -2\sqrt{3}\gamma k_z(k_x - ik_y), \quad I = -\sqrt{3}\gamma(k_x - ik_y)^2. \quad (\text{A1})$$

$$\hat{H}_L^\alpha = \frac{\hbar^2}{2m_0} \begin{pmatrix} Q^\alpha & H^\alpha & I^\alpha & 0 \\ (H^\alpha)^\dagger & -Q^\alpha & 0 & I^\alpha \\ (I^\alpha)^\dagger & 0 & -Q^\alpha & -H^\alpha \\ 0 & (I^\alpha)^\dagger & -(H^\alpha)^\dagger & Q^\alpha \end{pmatrix}, \quad Q^\alpha = -\frac{3}{5}\gamma(k_x^2 + k_y^2 - 2k_z^2), \quad H^\alpha = -\frac{4\sqrt{3}}{5}\gamma k_z(k_x - ik_y),$$

$$I^\alpha = \frac{\sqrt{3}\gamma}{5}(3k_x^2 + 4ik_x k_y - 3k_y^2). \quad (\text{A2})$$

It can be easily shown, that the first order correction to the hole ground state ($S_{3/2}$) energy in spherical NCs coming from \hat{H}_L^α calculated on the wave functions (15) is zero. The first order correction for cube-shaped NCs is already nonzero due to wave function structure. The Zeeman Hamiltonian (3) in matrix form is

$$\hat{H}_z = \mu_B \begin{pmatrix} -(3\kappa + \frac{27}{4}q)B_z & -(\sqrt{3}\kappa + \frac{7\sqrt{3}}{4}q)B_- & 0 & -\frac{3}{2}qB_+ \\ -(\sqrt{3}\kappa + \frac{7\sqrt{3}}{4}q) & -(\kappa + \frac{1}{4}q)B_z & -(2\kappa + 5q)B_- & 0 \\ 0 & -(2\kappa + 5q)B_+ & (\kappa + \frac{1}{4}q)B_z & -(\sqrt{3}\kappa + \frac{7\sqrt{3}}{4}q)B_- \\ -\frac{3}{2}qB_- & 0 & -(\sqrt{3}\kappa + \frac{7\sqrt{3}}{4}q)B_+ & (3\kappa + \frac{27}{4}q)B_z \end{pmatrix}, \quad (\text{A3})$$

where $B_\pm = B_x \pm iB_y$. The explicit form of orbital contribution $H_B = H_B^{\text{sph}} + \alpha H_B^\alpha$ neglecting quadratic on magnetic field terms of the isotropic part, H_B^{sph} , is

$$\hat{H}_B^{\text{sph}} = \mu_B \begin{pmatrix} P_B + Q_B & -S_B & R_B & 0 \\ -(S_B)^\dagger & P_B - Q_B & 0 & R_B \\ (R_B)^\dagger & 0 & P_B - Q_B & S_B \\ 0 & (R_B)^\dagger & (S_B)^\dagger & P_B + Q_B \end{pmatrix},$$

$$P_B = \gamma_1((zk_y - yk_z)B_x + (xk_z - zk_x)B_y + (yk_x - xk_y)B_z),$$

$$Q_B = \gamma((zk_y + 2yk_z)B_x + (2xk_z + zk_x)B_y + (yk_x - xk_y)B_z),$$

$$R_B = -\sqrt{3}\gamma_2(zk_y B_x - zk_x B_y + (yk_x - xk_y)B_z) + i\sqrt{3}\gamma_2(zk_x B_x - zk_y B_y + (yk_y - xk_x)B_z),$$

$$S_B = \sqrt{3}\gamma((xB_y - yB_x)(k_x - ik_y) + i(x - iy)k_z B_z - izk_z(B_x - iB_y)). \quad (\text{A4})$$

As we have shown, that to determine hole g factor components it is sufficient to calculate hole Zeeman splitting for $\mathbf{B}||z$. Here we show \hat{H}_B^{sph} components for $\mathbf{B} = (0, 0, B_z)$:

$$P_B = \gamma_1(yk_x - xk_y)B_z, \quad Q_B = \gamma(yk_x - xk_y)B_z,$$

$$R_B = -\sqrt{3}\gamma(ix(k_x + ik_y) + y(k_x - ik_y))B_z. \quad (\text{A5})$$

Note, that even H_B^{sph} can contribute to the anisotropic part of the hole effective g factor if the hole wave functions have

cubic symmetry in zero magnetic field.

$$\hat{H}_B^\alpha = \mu_B \begin{pmatrix} Q_B^\alpha & -S_B^\alpha & R_B^\alpha & 0 \\ -(S_B^\alpha)^\dagger & -Q_B^\alpha & 0 & R_B^\alpha \\ (R_B^\alpha)^\dagger & 0 & -Q_B^\alpha & S_B^\alpha \\ 0 & (R_B^\alpha)^\dagger & (S_B^\alpha)^\dagger & Q_B^\alpha \end{pmatrix},$$

$$Q_B^\alpha = -\frac{3\gamma}{5}((zk_y + 2yk_z)B_x + (2xk_z + zk_x)B_y + (yk_x - xk_y)B_z),$$

$$R_B^\alpha = -\frac{\sqrt{3}\gamma}{5}(-2iB_x zk_x - 3B_x zk_y + 3B_y zk_x + 2iB_y zk_y + 2iB_z xk_x - 3B_z yk_x + 3B_z xk_y - 2iB_z yk_y),$$

$$S_B^\alpha = -\frac{2\sqrt{3}\gamma}{5}((xB_y - yB_x)(k_x - ik_y) + i(x - iy)k_z B_z - izk_z(B_x - iB_y)). \quad (\text{A6})$$

If $\mathbf{B} = (0, 0, B_z)$, we have

$$Q_B^\alpha = -\frac{3\gamma}{5}((yk_x - xk_y)B_z),$$

$$R_B^\alpha = -\frac{\sqrt{3}\gamma}{5}(2ixk_x - 3yk_x + 3xk_y - 2iyk_y)B_z,$$

$$S_B^\alpha = -\frac{2i\sqrt{3}\gamma}{5}((x - iy)k_z B_z). \quad (\text{A7})$$

The matrix form of hole Zeeman effective Hamiltonian:

$$\hat{H}_Z^{\text{eff}} = \mu_B \begin{pmatrix} -\frac{3}{2}g_{3/2}^{\parallel}B_z & \frac{\sqrt{3}}{4}(3g_{3/2}^{\perp} - g_{1/2}^{\perp})B_- & 0 & -\frac{3}{2}g_{3/2}^{\perp}B_+ \\ \frac{\sqrt{3}}{4}(3g_{3/2}^{\perp} - g_{1/2}^{\perp})B_+ & -\frac{1}{2}g_{1/2}^{\parallel}B_z & -\frac{1}{2}g_{1/2}^{\perp}B_- & 0 \\ 0 & -\frac{1}{2}g_{1/2}^{\perp}B_+ & \frac{1}{2}g_{1/2}^{\parallel}B_z & \frac{\sqrt{3}}{4}(3g_{3/2}^{\perp} - g_{1/2}^{\perp})B_- \\ -\frac{3}{2}g_{3/2}^{\perp}B_- & 0 & \frac{\sqrt{3}}{4}(3g_{3/2}^{\perp} - g_{1/2}^{\perp})B_+ & \frac{3}{2}g_{3/2}^{\parallel}B_z \end{pmatrix}, \quad (\text{A8})$$

$g_{3/2}^{\parallel} = g_h + \frac{9}{2}Q^{\text{eff}}$, $g_{1/2}^{\parallel} = g_h + \frac{1}{2}Q^{\text{eff}}$, $g_{3/2}^{\perp} = Q^{\text{eff}}$, $g_{1/2}^{\perp} = 2g_h + 10Q^{\text{eff}}$. If the states with $|M| = 3/2$ and $1/2$ are split, the matrix elements of Hamiltonian (A8) mixing them with each other are zero and matrix Eq. (A8) can be separated into two independent matrices written in the basis of Bloch states u_{μ} with $\mu = +3/2, -3/2$ and $\mu = +1/2, -1/2$, correspondingly:

$$\hat{H}_Z^{\text{eff},3/2} = \mu_B \begin{pmatrix} -\frac{3}{2}g_{3/2}^{\perp}B_z & -\frac{3}{2}g_{3/2}^{\perp}B_+ \\ -\frac{3}{2}g_{3/2}^{\perp}B_- & \frac{3}{2}g_{3/2}^{\parallel}B_z \end{pmatrix}, \quad (\text{A9})$$

$$\hat{H}_Z^{\text{eff},1/2} = \mu_B \begin{pmatrix} -\frac{1}{2}g_{1/2}^{\parallel}B_z & -\frac{1}{2}g_{1/2}^{\perp}B_- \\ -\frac{1}{2}g_{1/2}^{\perp}B_+ & \frac{1}{2}g_{1/2}^{\parallel}B_z \end{pmatrix}. \quad (\text{A10})$$

In that case, each pair of states corresponding to the fixed M can be described by pseudospin $1/2$. In a spherically symmetric system, $g_{3/2}^{\perp} = Q^{\text{eff}} = 0$ and $g_{3/2}^{\parallel} = g_{1/2}^{\parallel} = g_{1/2}^{\perp}/2 = g_h$.

APPENDIX B: NUMERICAL CALCULATION OF HOLE ENERGIES, WAVE FUNCTIONS AND g FACTORS IN SPHERICAL NCs WITH INFINITE BOXLIKE POTENTIAL

We developed a numerical method for calculating hole energies, wave functions, and g factors in spherical NCs with infinite boxlike potentials, which is similar to our methods for spherical NCs with parabolic potential [31] and cube-shaped NCs with infinite boxlike potentials [11]. It consists of diagonalizing the hole Hamiltonian matrix, calculated on the basis of eigenfunctions of the Luttinger Hamiltonian in spherical approximation in spherical NCs with infinite boxlike potentials for a given set of Luttinger parameters γ_1, γ_2 and γ_3 in zero magnetic field [25] for full momentum j and its projection on the z -axis (15). For even solutions, the wave function for given values of j and M contains two contributions, with radial functions corresponding to l equal to $j - 3/2$ and $j + 1/2$, respectively [55] (we omit here the normalization constants):

$$R_{j,j-3/2}(r) = \sqrt{\frac{2j+3}{6j-3}} j_{j-3/2}(kr) - \frac{\sqrt{\frac{2j+3}{6j-3}} j_{j-3/2}(k) j_{j-3/2}(kr\sqrt{\beta})}{j_{j-3/2}(k\sqrt{\beta})}, \quad (\text{B1})$$

$$R_{j,j+1/2}(r) = \frac{(2j+3)j_{j-3/2}(k)j_{j+1/2}(kr\sqrt{\beta})}{(6j-3)j_{j-3/2}(k\sqrt{\beta})} + j_{j+1/2}(kr), \quad (\text{B2})$$

where $\beta = (\gamma_1 - 2\gamma)/(\gamma_1 + 2\gamma)$ is the light to heavy hole effective mass ratio and $j_l(x)$ are spherical Bessel functions. The equation determining the hole wave vector k comes from the boundary condition of the wave function vanishing at the

edge of the NC of radius a :

$$j_{j+1/2}(ka)j_{j-3/2}(\sqrt{\beta}ka) + \frac{(2j+3)j_{j-3/2}(ka)j_{j+1/2}(\sqrt{\beta}ka)}{6j-3} = 0. \quad (\text{B3})$$

For the odd states, the wave function for given values of j and M contains two contributions with l being equal to $j + 3/2$ and $j - 1/2$ and one has

$$R_{j,j-1/2}(r) = \sqrt{2j-1} j_{j-1/2}(kr) - \frac{\sqrt{2j-1} j_{j-1/2}(k) j_{j-1/2}(kr\sqrt{\beta})}{j_{j-1/2}(k\sqrt{\beta})}, \quad (\text{B4})$$

$$R_{j,j+3/2}(r) = \frac{(1-2j)j_{j+3/2}(kr)}{\sqrt{3}\sqrt{2j+3}} - \frac{\sqrt{3}\sqrt{2j+3}j_{j-1/2}(k)j_{j+3/2}(kr\sqrt{\beta})}{j_{j-1/2}(k\sqrt{\beta})}, \quad (\text{B5})$$

And from the boundary conditions one has

$$(2j-1)j_{j+3/2}(ka)j_{j-1/2}(\sqrt{\beta}ka) + 3(2j+3)j_{j-1/2}(ka)j_{j+3/2}(\sqrt{\beta}ka) = 0. \quad (\text{B6})$$

For the special case $j = 1/2$, the only one radial function remains:

$$R_{1/2,1}(r) = j_1(kr) \quad (\text{B7})$$

for even state and

$$R_{1/2,2}(r) = j_2(kr) \quad (\text{B8})$$

for the odd state, and with simple boundary conditions,

$$j_{l(2)}(ka) = 0 \quad (\text{B9})$$

for even (odd) states, correspondingly.

The introduced basis set is full, so one can use it for calculating hole states in a magnetic field. In addition, it allows valence band warping to be taken into account. In real world calculations, we use a finite size basis set, while choosing it to be sufficiently large for needed accuracy.

APPENDIX C: TRION EMISSION LINES IN AN APPLIED MAGNETIC FIELD

For a magnetic field oriented at an arbitrary angle θ with respect to the z axis of a NC, energies of the negative trion spin states are the eigenenergies of the hole Hamiltonian (A8). After the trion recombination, there remains an electron with a spin projection on the magnetic field direction $\pm 1/2$. In the case of the isotropic electron g factor, electron energy does

not depend on the angle θ and equals $\pm g_e \mu_B B/2$. Knowing energies of the excited and ground states, we can calculate energies for all possible trion emission lines.

To calculate the relative oscillator strength of the trion emission lines, we calculate the eigenvectors of the excited and ground states of a NC using the set of basis spin states along the z axis of the laboratory frame. The excited state of the system is described by eigenvectors of the Hamiltonian (A8). The dependence of the eigenvectors on the angle θ is described by the transformation matrix for spin 3/2 with

where $i, j = 1, 2, 3$, and 4 correspond to hole states with angular momentum projection $M = 3/2, 1/2, -1/2$, and $-3/2$ on the magnetic field direction and z axis, respectively. $i', j' = 1, 2$ correspond to electron states with spin projection $S = 1/2, -1/2$ on the magnetic field direction and z -axis, respectively. The matrices $T^{3/2}$ and $T^{1/2}$ are

$$T^{3/2} = \begin{pmatrix} \cos^3(\theta/2) & \sqrt{3} \cos^2(\theta/2) \sin(\theta/2) & \sqrt{3} \cos(\theta/2) \sin^2(\theta/2) & \sin^3(\theta/2) \\ -\sqrt{3} \cos^2(\theta/2) \sin(\theta/2) & \cos(\theta/2)(2 - 3 \cos^2(\theta/2)) & \sin(\theta/2)(2 - 3 \sin^2(\theta/2)) & \sqrt{3} \cos(\theta/2) \sin^2(\theta/2) \\ \sqrt{3} \cos(\theta/2) \sin^2(\theta/2) & -\sin(\theta/2)(2 - 3 \sin^2(\theta/2)) & \cos(\theta/2)(2 - 3 \cos^2(\theta/2)) & \sqrt{3} \cos^2(\theta/2) \sin(\theta/2) \\ -\sin^3(\theta/2) & \sqrt{3} \cos(\theta/2) \sin^2(\theta/2) & -\sqrt{3} \cos^2(\theta/2) \sin(\theta/2) & \cos^3(\theta/2) \end{pmatrix}, \quad (C3)$$

$$T^{1/2} = \begin{pmatrix} \cos(\theta/2) & \sin(\theta/2) \\ -\sin(\theta/2) & \cos(\theta/2) \end{pmatrix}. \quad (C4)$$

For a photon emitted along the z axis of the laboratory frame, we can calculate the relative oscillator strength of transitions between $|i\rangle$ and $|i'\rangle$ states. For this purpose, we use the following ratio between squared matrix elements of the operator $\mathbf{A}\mathbf{p}$, calculated on basis states along the z axis of NC:

$$\begin{aligned} |\langle j = \pm 3/2 | \mathbf{A}\mathbf{p} | j' = \pm 1/2 \rangle|^2 &\propto 3, \\ |\langle j = \pm 1/2 | \mathbf{A}\mathbf{p} | j' = \pm 1/2 \rangle|^2 &\propto 2, \\ |\langle j = \pm 1/2 | \mathbf{A}\mathbf{p} | j' = \mp 1/2 \rangle|^2 &\propto 1, \\ |\langle j = \pm 3/2 | \mathbf{A}\mathbf{p} | j' = \mp 1/2 \rangle|^2 &\propto 0. \end{aligned} \quad (C5)$$

Here, \mathbf{A} is the vector potential of electromagnetic field, \mathbf{p} is

good accuracy. For the ground state of the system, we use the transformation matrix for spin 1/2.

$$|i\rangle = \sum_{j=1}^4 T_{i,j}^{3/2}(\theta) |j\rangle, \quad (C1)$$

$$|i'\rangle = \sum_{j'=1}^2 T_{i',j'}^{1/2}(\theta) |j'\rangle, \quad (C2)$$

the momentum operator. Note that these selection rules are written for a negative trion with ground states composed of a resident electron. In the case of an electron-hole pair, the sign of the electron spin projection should be inverted.

The resulting intensities of the trion emission lines are calculated as

$$I_{i,i'} = \exp\left(-\frac{(E - \Delta E_{i,i'})^2}{2\sigma^2} - \frac{E_i}{kT}\right) |\langle i | \mathbf{A}\mathbf{p} | i' \rangle|^2. \quad (C6)$$

Here, the exponential prefactor takes into account broadening of trion lines with $\sigma = 0.05$ meV and Boltzman population of initial trion states with energies E_i .

- [1] A. L. Efros and L. E. Brus, Nanocrystal quantum dots: From discovery to modern development, *ACS Nano* **15**, 6192 (2021).
- [2] M. V. Kovalenko, L. Manna, A. Cabot, Z. Hens, D. V. Talapin, C. R. Kagan, V. I. Klimov, A. L. Rogach, P. Reiss, D. J. Milliron, P. Guyot-Sionnest, G. Konstantatos, W. J. Parak, T. Hyeon, B. A. Korgel, C. B. Murray, and W. Heiss, Prospects of nanoscience with nanocrystals, *ACS Nano* **9**, 1012 (2015).
- [3] L. Lv, S. Liu, J. Li, H. Lei, H. Qin, and X. Peng, Synthesis of weakly confined, cube-shaped, and monodisperse cadmium chalcogenide nanocrystals with unexpected photophysical properties, *J. Am. Chem. Soc.* **144**, 16872 (2022).
- [4] H. Lei, S. Liu, J. Li, C. Li, H. Qin, and X. Peng, Band-edge energy levels of dynamic excitons in cube-shaped CdSe/CdS core/shell nanocrystals, *ACS Nano* **17**, 21962 (2023).
- [5] D. Loss and D. P. DiVincenzo, Quantum computation with quantum dots, *Phys. Rev. A* **57**, 120 (1998).
- [6] S. Bosco, B. Hetényi, and D. Loss, Hole spin qubits in Si finfets with fully tunable spin-orbit coupling and sweet spots for charge noise, *PRX Quantum* **2**, 010348 (2021).
- [7] N. Piot, B. Brun, V. Schmitt, S. Zihlmann, V. P. Michal, A. Apra, J. C. Abadillo-Uriel, X. Jehl, B. Bertrand, H. Niebojewski, L. Hutin, M. Vinet, M. Urdampilleta, T. Meunier, Y.-M. Niquet, R. Maurand, and S. D. Franceschi, A single hole spin with enhanced coherence in natural silicon, *Nat. Nanotechnol.* **17**, 1072 (2022).
- [8] L. M. Roth, B. Lax, and S. Zwerdling, Theory of optical magneto-absorption effects in semiconductors, *Phys. Rev.* **114**, 90 (1959).
- [9] A. A. Kiselev, E. L. Ivchenko, and U. Rössler, Electron g factor in one- and zero-dimensional semiconductor nanostructures, *Phys. Rev. B* **58**, 16353 (1998).
- [10] A. Tadjine, Y.-M. Niquet, and C. Delerue, Universal behavior of electron g-factors in semiconductor nanostructures, *Phys. Rev. B* **95**, 235437 (2017).
- [11] M. A. Semina, A. A. Golovatenko, and A. V. Rodina, Influence of the spin-orbit split-off valence band on the hole g factor in semiconductor nanocrystals, *Phys. Rev. B* **104**, 205423 (2021).

- [12] J. M. Luttinger, Quantum theory of cyclotron resonance in semiconductors: General theory, *Phys. Rev.* **102**, 1030 (1956).
- [13] A. V. Malyshev, To the theory of magnetic-moment anisotropy of shallow acceptor centers in diamond-like semiconductors, *Phys. Solid State* **42**, 29 (2000).
- [14] B. L. Gel'mont and M. I. D'yakonov, g-factor of acceptors in semiconductors with the diamond structure, *Sov. Phys. Semicond.* **7**, 1345 (1973).
- [15] M. A. Semina and R. A. Suris, Holes localized in nanostructures in an external magnetic field: g-factor and mixing of states, *Semiconductors* **49**, 797 (2015).
- [16] A. L. Efros, M. Rosen, M. Kuno, M. Nirmal, D. J. Norris, and M. Bawendi, Band-edge exciton in quantum dots of semiconductors with a degenerate valence band: Dark and bright exciton states, *Phys. Rev. B* **54**, 4843 (1996).
- [17] E. Johnston-Halperin, D. D. Awschalom, S. A. Crooker, A. L. Efros, M. Rosen, X. Peng, and A. P. Alivisatos, Spin spectroscopy of dark excitons in CdSe quantum dots to 60 T, *Phys. Rev. B* **63**, 205309 (2001).
- [18] H. Htoon, S. A. Crooker, M. Furis, S. Jeong, A. L. Efros, and V. I. Klimov, Anomalous circular polarization of photoluminescence spectra of individual CdSe nanocrystals in an applied magnetic field, *Phys. Rev. Lett.* **102**, 017402 (2009).
- [19] L. Biadala, Y. Louyer, P. Tamarat, and B. Lounis, Band-edge exciton fine structure of single CdSe/ZnS nanocrystals in external magnetic fields, *Phys. Rev. Lett.* **105**, 157402 (2010).
- [20] F. Liu, L. Biadala, A. V. Rodina, D. R. Yakovlev, D. Dunker, C. Javaux, J. P. Hermier, A. L. Efros, B. Dubertret, and M. Bayer, Spin dynamics of negatively charged excitons in CdSe/CdS colloidal nanocrystals, *Phys. Rev. B* **88**, 035302 (2013).
- [21] C. Sinito, M. J. Ferrie, S. V. Goupalov, P. Mulvaney, P. Tamarat, and B. Lounis, Tailoring the exciton fine structure of cadmium selenide nanocrystals with shape anisotropy and magnetic field, *ACS Nano* **8**, 11651 (2014).
- [22] X. Marie, T. Amand, P. LeJeune, M. Paillard, P. Renucci, L. E. Golub, V. D. Dymnikov, and E. L. Ivchenko, Hole spin quantum beats in quantum-well structures, *Phys. Rev. B* **60**, 5811 (1999).
- [23] M. Syperek, D. R. Yakovlev, A. Grelich, J. Misiewicz, M. Bayer, D. Reuter, and A. D. Wieck, Spin coherence of holes in GaAs/(Al,Ga)As quantum wells, *Phys. Rev. Lett.* **99**, 187401 (2007).
- [24] M. Kugler, T. Andlauer, T. Korn, A. Wagner, S. Fehringer, R. Schulz, M. Kubová, C. Gerl, D. Schuh, W. Wegscheider, P. Vogl, and C. Schüller, Gate control of low-temperature spin dynamics in two-dimensional hole systems, *Phys. Rev. B* **80**, 035325 (2009).
- [25] B. L. Gel'mont and M. I. D'yakonov, Acceptor levels in diamond-type semiconductors, *Sov. Phys. Semicond.* **5**, 2191 (1971).
- [26] V. Kalevich and V. Korenev, Electron g-factor anisotropy in asymmetric GaAs/AlGaAs quantum well, *JETP Lett.* **56**, 253 (1992).
- [27] R. Winkler, *Spin-Orbit Coupling Effects in Two-Dimensional Electron and Hole Systems* (Springer, Berlin, 2003), p. 50.
- [28] G. Dresselhaus, A. F. Kip, and C. Kittel, Cyclotron resonance of electrons and holes in silicon and germanium crystals, *Phys. Rev.* **98**, 368 (1955).
- [29] G. L. Bir and G. E. Pikus, *Symmetry and Strain-Induced Effects in Semiconductors* (Wiley, New York, 1974).
- [30] E. I. Ivchenko, *Optical Spectroscopy of Semiconductor Nanostructures* (Alpha Science International Ltd., Harrow, UK, 2005).
- [31] M. A. Semina, A. A. Golovatenko, and A. V. Rodina, Ground State of the Holes Localized in II-VI Quantum Dots with Gaussian Potential Profiles, *Phys. Rev. B* **93**, 045409 (2016).
- [32] A. Baldereschi and N. O. Lipari, Spherical model of shallow acceptor states in semiconductors, *Phys. Rev. B* **8**, 2697 (1973).
- [33] A. Baldereschi and N. O. Lipari, Cubic contributions to the spherical model of shallow acceptor states, *Phys. Rev. B* **9**, 1525 (1974).
- [34] E. L. Ivchenko, *Optical Spectroscopy of Semiconductor Nanostructures* (Alpha Science, Harrow UK, 2005).
- [35] K. J. Vahala and P. C. Sercel, Application of a total-angular-momentum basis to quantum-dot band structure, *Phys. Rev. Lett.* **65**, 239 (1990).
- [36] P. C. Sercel and K. J. Vahala, Analytical formalism for determining quantum-wire and quantum-dot band structure in the multiband envelope-function approximation, *Phys. Rev. B* **42**, 3690 (1990).
- [37] A. R. Edmonds, *Angular Momentum in Quantum Mechanics* (Princeton University Press, Princeton, 1957).
- [38] A. L. Efros and M. Rosen, Quantum size level structure of narrow-gap semiconductor nanocrystals: Effect of band coupling, *Phys. Rev. B* **58**, 7120 (1998).
- [39] B. L. Gel'mont and A. V. Rodina, Energy representing binding of a hole to a multiply charged acceptor in semiconductors with the diamond structure, *Sov. Phys. Semicond.* **25**, 1319 (1991).
- [40] I. A. Merkulov and A. V. Rodina, Wave-functions and binding-energy of a hole in the ground-state of an acceptor in a diamond-like semiconductor, *Semiconductors* **28**, 195 (1994).
- [41] A. V. Malyshev, I. A. Merkulov, and A. V. Rodina, Ground-state wave functions of a non-Coulomb acceptor in diamond-like semiconductors, *Semiconductors* **30**, 91 (1996).
- [42] A. V. Malyshev, I. A. Merkulov, and A. V. Rodina, Theory of acceptor-ground-state description and hot photoluminescence in cubic semiconductors, *Phys. Rev. B* **55**, 4388 (1997).
- [43] H. Fu, L.-W. Wang, and A. Zunger, Applicability of the k-p method to the electronic structure of quantum dots, *Phys. Rev. B* **57**, 9971 (1998).
- [44] S. Adachi, *Handbook on Physical Properties of Semiconductors* (Springer US, 2004).
- [45] T. Friedrich, J. Kraus, M. Meininger, G. Schaack, and W. O. G. Schmitt, Zeeman levels of the shallow lithium acceptor and band parameters in cadmium telluride, *J. Phys.: Condens. Matter* **6**, 4307 (1994).
- [46] L. W. Molenkamp, R. Eppenga, G. W. 't Hooft, P. Dawson, C. T. Foxon, and K. J. Moore, Determination of valence-band effective-mass anisotropy in GaAs quantum wells by optical spectroscopy, *Phys. Rev. B* **38**, 4314 (1988).
- [47] A. V. Trifonov, I. A. Akimov, L. E. Golub, E. L. Ivchenko, I. A. Yugova, A. N. Kosarev, S. E. Scholz, C. Sgroi, A. Ludwig, A. D. Wieck, D. R. Yakovlev, and M. Bayer, Homogeneous optical anisotropy in an ensemble of InGaAs quantum dots induced by strong enhancement of the heavy-hole band Landé parameter g , *Phys. Rev. B* **104**, L161405 (2021).
- [48] M. V. Durnev, M. M. Glazov, E. L. Ivchenko, M. Jo, T. Mano, T. Kuroda, K. Sakoda, S. Kunz, G. Sallen, L. Bouet, X. Marie, D. Lagarde, T. Amand, and B. Urbaszek, Magnetic field induced

- valence band mixing in [111] grown semiconductor quantum dots, *Phys. Rev. B* **87**, 085315 (2013).
- [49] M. V. Durnev, Fine structure of electron-hole complexes in trigonal quantum dots, *Phys. Solid State* **57**, 1223 (2015).
- [50] S. Ithurria, M. D. Tessier, B. Mahler, R. P. S. M. Lobo, B. Dubertret, and A. L. Efros, Colloidal nanoplatelets with two-dimensional electronic structure, *Nat. Mater.* **10**, 936 (2011).
- [51] G. Qiang, A. A. Golovatenko, E. V. Shornikova, D. R. Yakovlev, A. V. Rodina, E. A. Zhukov, I. V. Kalitukha, V. F. Sapega, V. K. Kaibyshev, M. A. Prosnikov, P. C. M. Christianen, A. A. Onushchenko, and M. Bayer, Polarized emission of cdse nanocrystals in magnetic field: The role of phonon-assisted recombination of the dark exciton, *Nanoscale* **13**, 790 (2021).
- [52] E. Kirstein, D. R. Yakovlev, M. M. Glazov, E. A. Zhukov, D. Kudlacik, I. V. Kalitukha, V. F. Sapega, G. S. Dimitriev, M. A. Semina, M. O. Nestoklon, E. L. Ivchenko, N. E. Kopteva, D. N. Dirin, O. Nazarenko, M. V. Kovalenko, A. Baumann, J. Höcker, V. Dyakonov, and M. Bayer, The landé factors of electrons and holes in lead halide perovskites: Universal dependence on the band gap, *Nat. Commun.* **13**, 3062 (2022).
- [53] K. V. Kavokin and A. V. Koudinov, Dynamical polarization of nuclear spins by acceptor-bound holes in a zinc-blende semiconductor, *Phys. Rev. B* **88**, 235202 (2013).
- [54] <https://rscf.ru/en/project/23-12-00300/>.
- [55] A. I. Ekimov and A. A. Onushchenko, Size quantization of the electron energy spectrum in a microscopy semiconductor crystal, *JETP Lett.* **40**, 1136 (1984).